(1)

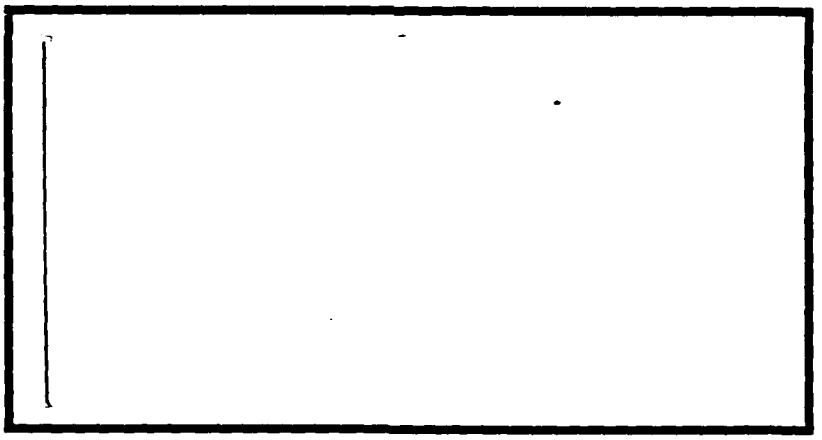

DEPARTMENT OF THE AIR FORCE

AIR UNIVERSITY

AIR FORCE INSTITUTE OF TECHNOLOGY

Wright-Patterson Air Force Base, Ohio

(1)

AFIT/GAE/AA/88D-23

EFFECT OF RIBLETS UPON FLOW SEPARATION IN A SUBSONIC DIFFUSER

THESIS

Nathan W. Martens
Captain, USAF

AFIT/GAE/AA/88D-23

AFIT/GAE/AA/88D-23

EFFECT OF RIBLETS UPON FLOW SEPARATION IN A SUBSONIC DIFFUSER

THESIS

Presented to the Faculty of the School of Engineering

of the Air Force Institute of Technology

Air University

In Partial Fulfillment of the

Requirements for the Degree of

Master of Science in Aeronautical Engineering

Nathan W. Martens, B.S.

Captain, USAF

December 1988

Preface

The study of the effect of riblets upon flow separation within a subsonic diffuser proved to be an interesting and challenging research project. As a result of this effort, I gained theoretical knowledge about such aerodynamic topics as turbulence, flow separation, diffusers, viscous drag reduction, and, of course, riblets. I also gained a vast amount of knowledge from the "hands on" experimental procedure employed during this project. Such experimental knowledge was gained through the design and fabrication of wind tunnel models, the operation of a low speed wind tunnel, and the set-up and calibration of all of the flow monitoring instrumentation.

I would like to recognize a number of individuals who made significant contributions to the completion of this research effort. First and foremost, I would like to thank Lt. Col. Paul I. King, my thesis advisor, whose knowledge and guidance were essential elements in the success of the project. I would also like to thank the other members of my thesis committee, Dr. W. C. Elrod and Dr. M. E. Franke, for their technical advise and inputs.

On a personal level, I would like to thank my wife and son whose patience and support were immeasurable during the rather difficult 18 months of study at AFIT. Lastly, I wish to dedicate this thesis to the memory of a true educator, my grandfather [redacted] who passed away during the course of my studies at AFIT. Not only was his whole life dedicated to the teaching of others, but he understood the great importance of making education practical and fun.

Nathan W. Martens

Table of Contents

List of Figures

List of Tables

List of Symbols

Symbol		Units
A	duct area	ft^2
A,B,C	hot film anemometer constants	None
A_e	diffuser area per unit width at boundary layer location	ft
dA_e/dx	area distribution per unit width	None
A_o	diffuser throat area per unit width at beginning of adverse pressure gradient	ft
c	Cole's integration constant (range 4.9 to 5.5)	None
C_D	drag coefficient	None
C_f	skin-friction coefficient	None
C_p	pressure coefficient	None
dC_p/dx	pressure distribution	None
D	drag on the surface	lbf
D_H	hydraulic diameter	ft
E	bridge voltage	volts
F(x)	Stratford's criteria separation parameter	None
H	one half of the diffuser throat width	ft
h	riblet peak-to-valley height	ft
h^+	nondimensional riblet peak-to-valley height	None
L	diffuser wall length	ft
M	water manometer reading	in.
P	mercury barometer barometric pressure	in.
p	duct perimeter	ft
Re	Reynolds number, $Re = UD_H/\nu$	None
R_x, Re_x	Reynolds number, $R_x = Re_x = U_e x/\nu$	None
Re_{sep}	Reynolds number, $Re_{sep} = (UD_H)_{sep}/\nu$	None
Re_{th}	Reynolds number, $Re_{th} = (UD_H)_{th}/\nu$	None
s	riblet peak-to-peak width	ft
s^+	nondimensional riblet peak-to-peak width	None
T	absolute temperature (Fahrenheit)	F
U	flow velocity, freestream velocity	ft/sec

U_e	boundary layer edge velocity	ft/sec
U_o	velocity at beginning of adverse pressure gradient .	ft/sec
U_{sep}	velocity at diffuser flow separation location	ft/sec
U_{th}	diffuser throat velocity	ft/sec
U_τ	friction velocity	ft/sec
u	local flow velocity	ft/sec
u^+	dimensionless velocity parameter	None
V	diffuser throat velocity (figures only)	ft/sec
W	diffuser throat width, W = 2H	ft
w	surface width, diffuser model width	ft
$w(y/\delta)$	Cole's wake function	None
x	horizontal location along the surface (flat plate) .	ft
x	flow location measured from the minimum pressure point	ft
x_{sep}	flow separation location measured from the minimum pressure point	ft
Δx_{sep}	difference in flow separation location	ft
y	local vertical height	ft
δ	boundary layer thickness	ft
ϵ	error parameter	None
ϵ_{rms}	root-mean-square-error value	None
η	Blasius solution flow constant	None
θ	one half of the diffuser divergence angle	deg
2θ	diffuser divergence angle	deg
κ	von Karman's mixing-length constant	None
ν	kinematic viscosity	ft^2/sec
$\Pi(x)$	Cole's profile parameter	None
ρ	fluid density	$slugs/ft^3$
$\phi_1(y^+)$	turbulent boundary layer law-of-the-wall function ..	None

Abstract

The objective of this thesis was to investigate the effect of riblets upon flow separation in a two-dimensional straight-walled subsonic diffuser. Riblets are small flow-aligned grooves which can be attached to an aerodynamic body. Studies involving the application of riblets to turbulent flow over a flat plate have consistently shown a decrease in viscous drag as compared to the same surface without riblets. The purpose of this investigation was to determine the effect applying riblets to the walls of a subsonic diffuser would have upon flow separation in the fluid handling device.

For this investigation, it was found flow separation was indeed delayed in a diffuser employing riblets as compared to a geometrically identical plain diffuser. For the smaller throat widths, this delay was significant, being as high as 250% due to riblets. As the diffuser throat width increased, the delay in flow separation due to riblets decreased. Also evident in the investigation was the strong dependence of flow separation upon throat velocity for the diffuser with riblets.

EFFECT OF RIBLETS UPON FLOW SEPARATION IN A SUBSONIC DIFFUSER

I. Introduction

The primary purpose of this thesis was to experimentally investigate the effect of riblets upon flow separation in a subsonic diffuser. Riblets are small longitudinally oriented grooves that can be attached to an aerodynamic or hydrodynamic surface. They were originally introduced in 1979 as a passive technique for reducing viscous drag over a body subjected to turbulent flow (1:168). This thesis employed a subsonic diffuser as the test model because of its susceptibility to the production of an adverse pressure gradient resulting in flow separation. Basically, this research effort involved subjecting riblets to a turbulent boundary layer adverse pressure gradient and determining the impact upon the location of flow separation within a subsonic diffuser section.

Background

Viscous fluid flow can be characterized as being laminar, turbulent, or in a transitional state between the two. Laminar flow defines the condition where the fluid flow is smooth and orderly. The flow is steady with basically parallel layered streamlines. In a duct, laminar flow usually occurs when the Reynolds number is less than 2000. The other distinct type of viscous fluid flow is turbulent flow. The turbulent flow regime is characterized as having irregular, unsteady, and disorderly motion of subsections of fluid within the flowing medium. It

usually occurs at Reynolds numbers greater than 2000. Hinze (2:2) defines turbulence as "... an irregular condition of flow in which various quantities show a random variation with time and space coordinates, so that statistically distinct average values can be discerned." The key items in this definition are that turbulence is random in time and space, and its properties, such as velocity and pressure, can be time averaged at distinct points in the flow. The ability to average turbulence quantities exists because turbulent flow consists of a distinctive pattern, repeating at regular intervals in time and space within the domain being considered (2:4). On a basic level, the turbulent flow pattern is composed of an infinite number of eddies or vortices confined within a distinct, albeit irregular, three dimensional boundary. Each eddy contains a specific amount of kinetic energy, depending upon its size, and a corresponding rotational velocity.

There are a number of unique characteristics associated with the distinctive structure of turbulence. The first of these characteristics deals with diffusiveness. In turbulence, transferable flow properties are diffused by the interaction of the eddies, whereas in laminar flow diffusion occurs through molecular motion. The eddy viscosity associated with turbulent flow is much larger than the molecular viscosity corresponding to laminar flow. The larger the viscosity within the flow, the greater its diffusion rate. Therefore, turbulent flow, having a greater effective viscosity than laminar flow, has a correspondingly higher diffusiveness. Experimentally, the difference in the diffusion rate between the two flows has been shown to be a factor of 20 (3:27).

As a result of its extreme diffusiveness, a turbulent flow experiences a greater amount of momentum transport to and from a surface

within the flow regime. The amount of the momentum transfer in the flow directly correlates to the value of skin friction or viscous drag of the boundary layer on a surface. The large transport of momentum in turbulent flow manifests itself as a high value of viscous drag and vice versa. Therefore, the second characteristic of turbulence is that turbulent boundary layers can produce values of viscous drag twice those of laminar boundary layers (4:14).

One prevalent problem of viscous fluid flow is the occurrence of flow separation. When the flow separates from a surface, losses may occur which are detrimental to component performance. For subsonic external flow, such as flow over an airfoil, separation physically causes a deviation in the streamlines, a reversal in the flow direction, and stalling (5:2). The losses associated with stall appear as an increase in drag and a decrease in lift. For internal flows, such as flow through a diffuser, separation reduces the efficiency of the fluid handling device (5:2).

One of the main contributors to flow separation is viscosity. According to Prandtl's boundary layer concept (6:40), "... at high Reynolds numbers the effects of viscosity are confined to a very thin layer close to the body and a thin wake extending from the body." Due to viscosity, the velocity of the fluid at the surface of a body is zero. As the normal distance from the surface increases through the boundary layer, the effects of viscosity diminish and the flow velocity increases. One characteristic of the boundary layer is that when proper conditions exist, the flow near the body can reverse direction and move backwards as compared to the freestream flow direction. Due to this reverse flow, the boundary layer usually separates resulting in the

separation of the main flow from the body.

In order for this reverse flow condition at the body surface to exist, the pressure at the wall must increase in the same direction as the freestream. The existence of this positive pressure gradient, referred to as an adverse pressure gradient, causes the onset of reverse flow at the surface resulting in the separation of the boundary layer and the main flow. Therefore, it can be stated "... that separation of the boundary layer results from an adverse pressure gradient" (6:50).

As discussed, the two necessary and sufficient conditions for flow separation are the presence of viscosity and an adverse pressure gradient. Even though the turbulent boundary layer has a higher effective viscosity than the laminar boundary layer, the highly diffusive nature of turbulence allows it to delay flow separation. Because of its greater diffusiveness, the large momentum transfer associated with turbulent flow actually resists separation. Therefore, turbulent flows can delay the onset of flow separation as compared to laminar flows. When dealing with turbulence, one must consider the trade-off between the enhanced capability to delay separation with the associated penalty of an increase in viscous drag.

A diffuser is a device used to decelerate fluid flow. In the design of aircraft engines, this is an important function. For turbojet engines, a diffuser is used as part of the air intake duct to slow the flow entering the compressor to a Mach number of 0.4 or less (7:191). Diffusers are also used to alter "... the flow entering the main burner where the flow leaving the compressor must be slowed from a high subsonic Mach number to a very low Mach number. Another instance is the flow entering the afterburner where the flow leaving the turbine must be

slowed from a high subsonic Mach number to a Mach number of about 0.2" (8:305).

Physically, a subsonic diffuser consists of diverging walls that act as a channel for fluid flow. As the flow is decelerated within the channel, kinetic energy is converted to pressure energy. How well this conversion of energy is performed basically determines the overall efficiency of the diffuser. It is also important for the flow leaving the diffuser to be uniform in order to reduce distortions in the velocity profile which can disturb the aerodynamics of downstream machine components (7:191). The combination of energy conversion efficiency and flow uniformity determines the overall contribution to the performance of the machinery (such as an aircraft engine) of which the diffuser is but one component.

One characteristic of diffuser flow is that since the flow is being decelerated, an adverse pressure gradient exists creating the possibility of flow separation from the walls (8:305). Flow separation has a devastating impact upon diffuser performance. A separated flow greatly reduces the efficiency of the energy conversion process. "The conversion of kinetic energy to pressure energy may take place with loss of energy because of viscous effects of fluids involving the flow separation" (5:158). A reduction in the efficiency of the energy conversion process directly correlates to a decrease in the overall effectiveness and efficiency of the diffuser flow. A physical example of where the disadvantages of separation can occur involves the flow through an aircraft engine inlet. Separation in the diffusing section of an engine inlet reduces the recovery of total pressure, thus reducing the thermal efficiency of the engine.

In many cases, diffuser flow is turbulent (5:158). Being turbulent, the flow is better able to resist separation than if it was laminar. However, the turbulent flow separation point within the diffuser can be more than just a function of the viscosity in the flow. Chang (5:161) reports that experiments conducted by Polzin (5:161) showed that geometrically similar diffuser sections also produced different locations of flow separation depending upon wall roughness. Surface separation occurred earlier in the diffuser sections with rough walls as compared to those with smooth walls (5:161-162). This indicates that when friction is reduced, flow remains attached farther downstream. It seems that if the flow can be made to remain turbulent but with a smaller friction coefficient, attachment is enhanced.

Recent studies in the area of viscous drag reduction have included the use of passive means to control turbulent boundary layers (4:14,16; 9:24-27; 10:1-8). One such method employed is to use riblets: small, flow aligned, longitudinally grooved surfaces, usually V-shaped, with varying optimum peak-to-valley heights depending upon the flow velocity (9:26). Riblets can be purchased as a thin film which is adhesively mounted on the desired surface. A number of studies involving the use of riblets on flow over a flat plate have consistently shown a decrease in viscous drag as high as 8% compared with the same surface without riblets (10:1,4; 11:1,4,7). This reduction in viscous drag is primarily attributed to the ability of riblets to control and damp turbulence, thereby reducing turbulent shear.

Objective

The primary objective of this thesis was to study the effect of

riblets on flow separation in a subsonic diffuser. The scope of the experimental research involved determining whether the predicted reductions in viscous drag due to the application of riblets would alter the location of flow separation in a two-dimensional straight-walled subsonic diffuser. It was expected that viscous drag on the walls of a diffuser section would be reduced by applying riblets, as a result of retarding the near wall adverse pressure gradient effect, thereby delaying the onset of flow separation.

II. Theory

The primary emphasis of this thesis was directed at the study of riblets and diffuser flow. Riblets were investigated because of their proven ability to reduce viscous drag in turbulent flow. Diffuser flow was studied because of its inherent nature to generate an adverse pressure gradient which, when strong enough, can lead to flow separation.

Riblets

Since their introduction in the late 1970's, riblets have become one of the most consistent and relatively easy ways to reduce viscous drag. Even though riblets considerably increase wetted surface area, numerous studies have shown riblets can reduce viscous drag on a surface by as much as 8% (10:1,4; 11:1,4,7). However, riblets are only effective in reducing skin friction drag over surfaces subjected to turbulent flow. Therefore, the underlying theory of riblets involves an understanding of their impact upon the turbulent boundary layer.

Anders, Walsh, and Bushnell (9:27) describe the production of drag within a turbulent boundary layer as follows:

> Most of the drag produced by a turbulent boundary layer originates from unsteady events occurring randomly in time and space. A widely accepted view is that these events, termed bursts, are part of a quasiordered series of events that begins with a low-speed region between a pair of counter-rotating longitudinal vortices near the wall. According to this view, some unidentified triggering mechanism forces this low-speed fluid away from the wall to a higher velocity region in the boundary layer where a shear-layer instability oscillates and eventually breaks up the low-speed streak. By some estimates the breakup event is responsible for 70-80% of the skin friction under a turbulent boundary layer.

A conceptual model of the process just described is given by Hooshmand, Wallace, and Balint (12:1). They describe the turbulence over a surface

as "...a 'hairpin'-like vortex which is formed by the vorticity diffusing from the wall which is lifted away from it and stretched downstream by the main shear" (12:1). Such a stretched vortex is referred to as a streak. This process is characterized by "...the 'bursting' of low momentum fluid away from the wall and the 'inflow' of high momentum fluid back towards the wall ..." (12:1). This transition of fluid to and from the wall is a very effective means of transporting momentum and heat, and accounts for the majority of the boundary layer surface drag.

The skin friction reduction capability of riblets seems to be related to their ability to alter the "hairpin"-like vortices associated with the turbulent boundary layer structure. The interaction of riblets with the counter-rotating streamwise vortices of turbulence results in the generation of a secondary vortex which begins at the riblet peak and extends down into the riblet valley as shown in Figure 1 (13:1384).

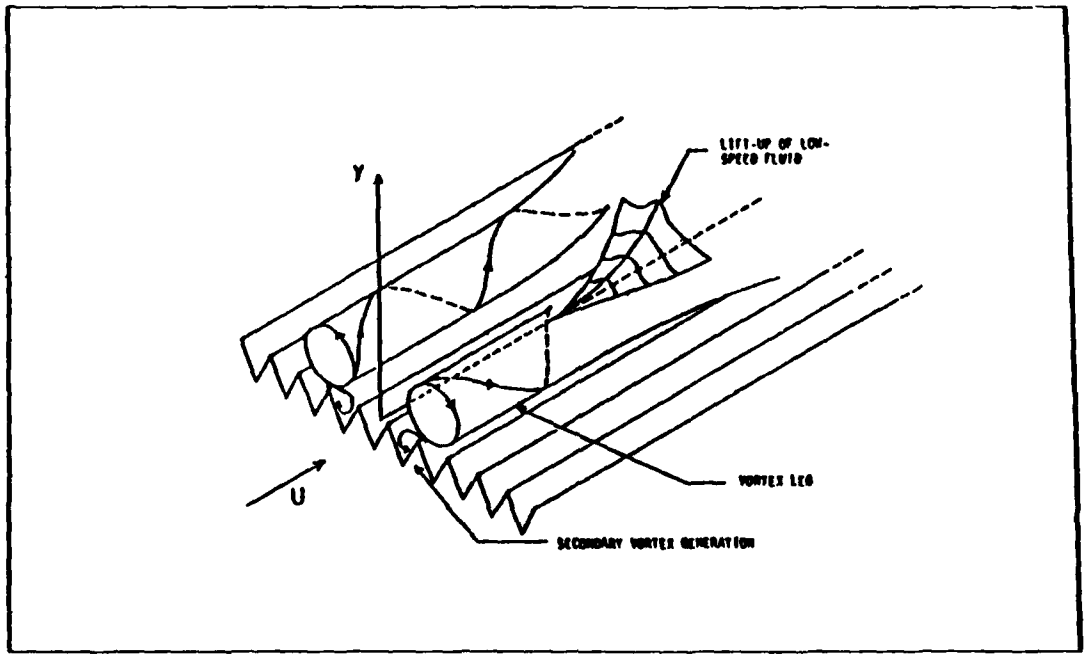

Fig. 1. Secondary Vortex Generation on a Riblet Surface (13:1384)

As these secondary vortices are generated, the primary streamwise vortices are weakened. Experiments have shown the streamwise turbulence intensity is reduced by approximately 15% due to the introduction of secondary vortices into the flow structure (12:1). Also, the presence of the secondary vortices acts to inhibit the transition of "... the spanwise concentration of low-speed fluid into streak formations" (13:1384). Stated another way, the secondary vortices increase spanwise streak spacing. Experiments have shown this increase in spanwise streak spacing to be as much as 40% over the spacing detected in flat plate flows (14:1). By inhibiting streak formation, the number of sites where "bursting" of low momentum fluid away from the wall occurs is decreased, thereby reducing the exchange of momentum within the boundary layer (13:1384). This reduction in momentum transfer tends to retard the development of the turbulent boundary layer on the riblet surface. By reducing both the streamwise intensity and momentum transfer of the turbulent boundary layer, riblets are capable of reducing viscous drag on a surface. Physically, riblets inhibit turbulent momentum transport resulting in the generation of "... a relatively quiescent flow in the riblet valley that pushes skin-friction-producing turbulence up and away from the surface" (9:26).

One very important parameter controlling the ability of riblets to reduce viscous drag is their size. The dimensions of the longitudinal grooves in relation to the size of the turbulent boundary layer formed on the surface has a direct impact upon the viscous drag reducing capability of the riblets. "According to experimental data, a turbulent boundary layer can be regarded approximately as a composite layer made up of inner and outer regions. The existence of the two regions is due to the

different response to shear and pressure gradient by the fluid near the wall" (3:91-92). The inner region of the boundary layer can be subdivided into three layers consisting of the viscous laminar sublayer, the transitional region, and the fully turbulent region (3:94,95). In order for riblets to generate the secondary vortices responsible for reducing viscous drag (see Figure 1), they must extend through the viscous laminar sublayer into the transitional region of the turbulent boundary layer inner region. However, if the grooves are too large, the skin friction drag corresponding to the increased wetted area will counteract the viscous drag reducing capability of the riblets and may actually increase the overall surface drag (9:26,27).

The two nondimensional parameters affecting riblet performance are the peak-to-valley height (h^+) and the peak-to-peak width (s^+). These two parameters are defined as follows (11:1):

$$h^+ = hU_\tau/\nu \tag{1}$$

$$s^+ = sU_\tau/\nu \tag{2}$$

where

h^+ = nondimensional riblet peak-to-valley height
h = riblet peak-to-valley height (ft)
U_τ = friction velocity (ft/sec)
ν = kinematic viscosity (ft^2/sec)
s^+ = nondimensional riblet peak-to-peak width
s = riblet peak-to-peak width (ft)

A number of studies have shown that the maximum drag reduction for V-groove geometry riblets applied to a flat plate occurs for h^+ values between 8 and 15 (15:3; 16:485). Furthermore, riblets continue to show the ability to reduce drag for values of h^+ up to 30 (1:168; 16:485;

17:134). From Equation 1, the optimal riblet size can be determined by using the following relationship:

$$h = h^{+}\nu/U_{\tau} \tag{3}$$

The optimal riblet size corresponds to setting h^{+} to a value between 8 and 15 in Equation 3. Since the kinematic viscosity is basically a constant, dependent upon the type of fluid flow (air or water) and the temperature, the friction velocity, U_{τ}, is the only parameter that needs to be calculated in Equation 3 to determine the optimum h. The friction velocity is defined as follows (11:1):

$$U_{\tau} = U_{e} \, (C_{f}/2)^{1/2} \tag{4}$$

where

U_{e} = boundary layer edge velocity (ft/sec)
C_{f} = skin-friction coefficient

The skin-friction coefficient, C_{f}, parameter is dependent upon the roughness of the surface over which the flow is passing and is determined from non-riblet measurements. For V-groove shaped riblets, the maximum viscous drag reduction is achieved by equating s to the calculated value for h (17:134-135).

Diffuser

As stated in the Introduction, the purpose of a subsonic diffuser is to provide slowed and undistorted flow to such mechanical devices as an aircraft engine compressor or afterburner. In principle, a subsonic diffuser converts dynamic pressure (kinetic energy) into static pressure (pressure energy) by decelerating the flow through an expanding channel. The overall effectiveness of a diffuser is determined by the level of

efficiency it achieves in performing this energy conversion process. As it pertains to an aircraft propulsion system, the higher the total pressure recovery of the flow leaving a diffuser, the greater the thermal efficiency of the engine. Enhancing engine thermal efficiency results in greater thrust output while reducing fuel consumption, thereby improving the overall performance of an aircraft. In addition to the efficient conversion of energy, it is also important that the flow exiting a diffuser be uniform and steady. Distortions in the exit flow can degrade the performance of downstream aircraft engine components.

The basic principle involved in designing a diffuser for an aircraft "... is to define the duct geometry that will provide the highest performance for given airframe constraints and diffuser entrance conditions" (18:2). Two primary parameters in determining the flow behavior through a diffuser are the divergence angle (2θ) and the ratio of wall length to throat width (L/W). When the design of these two parameters is optimized, the flow is well-behaved with a high total pressure recovery. However, when geometric and weight constraints (which are common in aircraft design) prevent design optimization, flow separation and stall can occur in the diffuser section. Figure 2 (19:307) shows the flow regimes associated with different combinations of 2θ and L/W for two-dimensional straight-walled diffusers. Flow separation in a diffuser greatly diminishes its efficiency. "The static pressure gradient decreases and the mixing losses increase rapidly" (7:192). The mixing results in the reduction of the average stagnation pressure of the stream because energy is lost as the slower and faster portions of the flow interact (7:194). In addition to low pressure recovery, stalled flow results in "... severe flow asymmetry, severe

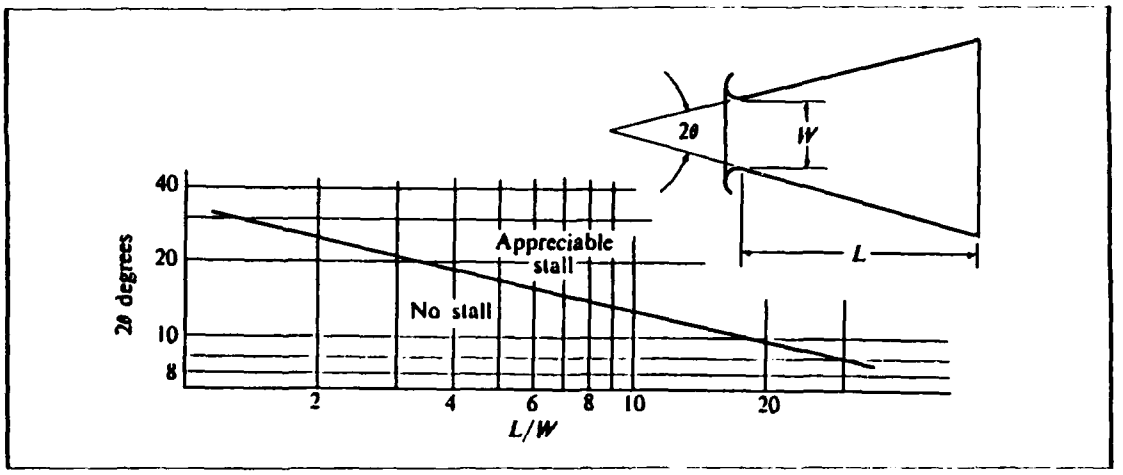

Fig. 2. Flow Separation Regimes for Straight-Walled Diffusers (19:307)

unsteadiness, or both" (20:141).

Since the flow is slowing as it passes through a subsonic diffuser, the adverse pressure gradient can cause the flow to reverse directions at the diffuser surface. It is this region of reversed flow that causes the main stream to separate from the surface and stall. Bower (18:3,4) describes the impact of the adverse pressure gradient upon diffuser flow as follows:

> At the entrance plane of the duct, the boundary layer, which is generally turbulent, is relatively thin, and the velocity profile is typical of the 1/7-power-law variation. As the air stream moves against the adverse pressure gradient, which is nearly constant across any section of the boundary layer, it is retarded by the force of the pressure gradient and by friction at the bounding wall. When the momentum of the boundary layer is no longer able to overcome these forces and the fluid near the wall is brought to rest, the boundary layer separates. At the point of separation, the wall shear stress vanishes, and the inflection point appears in the boundary layer velocity profile. As the flow continues to oppose the adverse pressure gradient, the fluid near the wall begins to flow in the opposite direction to the mainstream. Due to this reversal, a zero-velocity surface is established within the diffuser as well as along the wall, and the fraction of the channel cross-sectional area in which viscous effects are important becomes increasingly larger.
>
> The strength of the adverse pressure gradient found in a diffuser

depends on 2θ and L/W. As shown in Figure 2, increasing 2θ and L/W will increase the adverse pressure gradient strength enough to stall the flow. However, as stated in the Introduction, a higher freestream turbulence intensity will increase the momentum transfer through the boundary layer to the surface, thereby delaying flow separation.

Depending upon the strength of the adverse pressure gradient, four different flow regimes can be found in a diffuser. With increasing adverse pressure gradient strength, the four flow regimes encountered are as follows: "... (a) unstalled flow, (b) transient, three-dimensional stalls, (c) steady, two-dimensional stalls, and (d) jet flow separated from both walls" (21:1). The first flow regime (unstalled flow) is found at small 2θ and L/W values. The flow is well-behaved with no main stream separation. As 2θ and L/W are increased, the second region of flow is encountered. This regime is characterized by a "... region of large transitory stall in which the separation varies in position, size, and intensity with time. This is a regime of highly pulsating flows" (22:322). The steady, two-dimensional stall zone is characterized by a large fixed region of turbulent flow recirculation along one wall of the diffuser. Flow along the other diffuser wall remains attached and basically steady. The final separated flow regime occurs when the divergence angle is very large. Referred to as jet flow, this zone is characterized by the detachment of the flow from both diffuser walls reducing the main stream to only a small region in the middle of the diffuser section. These four distinct regions of flow alter the performance of a diffuser. "Overall pressure recovery and efficiency are high in the unstalled regime and drop only a small amount through the three-dimensional-stall zone, but they drop to very low values as soon as

two dimensional steady separation begins" (21:2). In the jet flow regime "... practically no static pressure rise takes place in the diffuser" (7:193).

Studies have shown that surface roughness or wall skin friction affect the location of flow separation in subsonic two-dimensional diffusers. Experiments conducted with geometrically similar diffusers showed that surface separation and stall occurred farther upstream on channels with rough walls as compared to those with smooth walls (5:161). Rough surfaces increased the amount of the turbulent boundary layer energy lost to friction causing boundary layer stall, with the resultant separation of the main stream, to occur earlier on the diffuser wall.

As it pertains to this thesis, it is felt the application of riblets to the wall of a diffuser can affect the location of flow separation within the expanding channel. It is hypothesized that the viscous drag reduction capability of riblets will act similar to smoothing the walls of a diffuser. By reducing the skin friction drag, the turbulent boundary layer energy usually lost to viscosity will be reduced, thereby delaying boundary layer stall. Also, the formation of the wall reversed flow should be slowed due to the reduction in viscous drag, resulting in the delay of flow separation. Since riblets decrease streamwise turbulence intensity, they do not disturb, but should actually enhance, the stabilization of the flow. Such stabilization satisfies the requirement for the flow exiting a diffuser to be undistorted.

Flow Separation

There are a variety of ways the location of internal flow separation

can be determined. This thesis employed a visualization and a numerical method to locate the position of main stream separation from the diffuser wall. The visualization method consists of applying some type of substance to the diffuser surface such as oil drops or tufts of string. When the oil drops streak or the string flutters, this indicates the presence of flow on the surface. Oil drops that remain circular or string lying motionless indicates the absence of flow on the surface. In this way, flow separation can be determined by observing the behavior of an applied substance on a body's surface. In this thesis, both the oil drop and string tuft methods were employed to determine the flow separation by visualization.

The numerical method used for predicting the location of flow separation was Stratford's criteria. In a study conducted by Cebeci (3:202), the Stratford method was found to be very accurate in predicting the separation point in turbulent flows. The Stratford method consists of using the following equation to predict separation (3:204):

$$C_p \left[x(dC_p/dx)\right]^{1/2} (10^{-6}R_x)^{-1/10} = F(x) \qquad (5)$$

where

C_p = pressure coefficient, $C_p = 1 - (U_e/U_o)^2$
x = flow location measured from the minimum pressure point (ft)
dC_p/dx = pressure distribution
R_x = Reynolds number, $R_x = xU_e/\nu$
U_e = boundary layer edge velocity (ft/sec)
U_o = velocity at beginning of adverse pressure gradient (ft/sec)
$F(x)$ = Stratford's criteria separation parameter

Equation 5 "... assumes an adverse pressure gradient starting from the leading edge, as well as fully turbulent flow everywhere" (3:204). In

the case of a diffuser, the equation assumes that the adverse pressure gradient forms at the beginning of the expanding channel. Equation 5 was modified using the continuity equation for steady one-dimensional incompressible fluid flow and the geometry of the diffuser. This procedure is discussed in detail in Appendix C. The modification resulted in Equation 6 shown below:

$$F(x) = [1 - H^2/(H + x\tan\theta)^2][2xH^2\tan\theta/(H + x\tan\theta)^3]^{1/2}(R_x 10^{-6})^{-1/10} \quad (6)$$

where

H = one half of the diffuser throat width (ft)
θ = one half of the diffuser divergence angle (deg)

This equation was used in the thesis to predict flow separation in a diffuser. "For a typical turbulent boundary-layer flow with an adverse pressure gradient, it is found that F(x) increases as separation is approached and decreases after separation" (3:205). According to Stratford (3:205), "... if the maximum value of F(x) is (a) greater than 0.40, separation is predicted when F(x) = 0.40; (b) between 0.35 and 0.40, separation occurs at the maximum value; (c) less than 0.35, separation does not occur." The procedure used in this thesis was to iterate x with respect to F(x) and determine the separation location according to Stratford's criteria stated above.

III. Experimental Apparatus

Wind Tunnel

The experimental research for this thesis was conducted in the Air Force Institute of Technology Nine Inch Wind Tunnel Facility located in Building 640, Area B, of Wright-Patterson AFB. The facility consists of a low speed, open circuit, draw-down wind tunnel and its supporting power supply. The wind tunnel test section has a 9 by 9 in. square cross section and is 37 in. long. The floor and ceiling of the test section are constructed of wood and both side panels are made of plexiglass. The side panels are hinged at the top for upward opening accessibility to the test section. Seven circular instrumentation access ports, spaced 5 in. apart, are located along the centerline of the test section floor and ceiling. The ceiling access holes have a 1.5 in. diameter and the floor ports are 0.25 in. in diameter.

The flow velocity through the wind tunnel was measured using a 2 in. inclined water manometer manufactured by Dwyer Instruments. The manometer was attached to four manifold pressure ports, one located at the midpoint of each wall of the tunnel just in front of the test section. This pressure port arrangement allowed for an average static pressure reading to be taken across the entire cross section of the wind tunnel. One end of the manometer was open to room atmosphere, the pressure of which is the tunnel total pressure, within 0.5%. Along with the manometer reading, temperature and barometric pressure values were required in order to calculate flow velocity. A digital thermometer was mounted in the aft end of the test section to provide accurate

temperature readings to a tenth of a degree, Fahrenheit. The barometric pressure was read, in inches of mercury, from a wall mounted barometer located in the same room as the wind tunnel. The maximum tunnel velocity achieved during experimentation was 63 ft/sec.

Anemometry System

A hot film anemometry system was used to determine the characteristics of the freestream flow and surface boundary layers. Specifically, a hot film anemometer was used to measure the velocity over the bodies investigated in this thesis. The anemometry system consisted of an IFA 100 System Intelligent Flow Analyzer, Model 1218-20 Hot Film Boundary Layer Probes, and an 18 in. single sensor anemometer probe holder. All three items were manufactured by Thermo-Systems Incorporated. The IFA 100 displays hot wire/film anemometer readings as bridge voltage which can be correlated to flow velocity. The Model 1218-20 Boundary Layer Probe has a hot film sensor measuring 0.002 in. in diameter. The boundary layer probe is constructed with a small metal rod extending from its base designed to protect the hot film from contacting the surface. The distance between the end of the protecting rod and the hot film is 0.005 in. An 18 in. single sensor probe holder was used to connect the hot film anemometer to the IFA 100. The probe holder was attached to a manual traversing mechanism that could be inserted into any one of the five instrumentation holes located in the ceiling of the tunnel test section. The traversing mechanism employs a vernier scale to measure distance in the y-direction.

Once the anemometry system was connected, a square wave test signal, located internally to the IFA 100, was applied to the bridge of the hot

film sensor in order to visually optimize the anemometer's frequency response (23:2-3). A Model 1570A Dual Time Base Oscilloscope, manufactured by B-K Precision, was connected to the IFA 100 to provide the required visualization of the test signal.

Tunnel Models

Two wind tunnel models were used in the performance of the thesis experimental research. The first model was a flat plate and the second one was an adjustable diffuser section.

The flat plate model was constructed of aluminum and measured 18 in. in length, 8.9 in. in width, and had a thickness of 0.0625 in. The leading edge was cut at a 15 deg angle. This cut provided the flat plate with a sharp leading edge (later determined to be a problem). The model was mounted on a single aluminum support stand mounted below the plate, 8.5 in. from the leading edge.

After initial measurements were made, a number of modifications were needed to correct flow problems. The first of these modifications was the addition of an inclined flap to the aft end of the plate. This flap was constructed of aluminum and measured 6 in. in length, 8 in. in width, and had a thickness of 0.0625 in. It was mounted 15.25 in. from the plate leading edge and was deflected a fixed value of 30 deg from the plate surface. The flap was attached to the flat plate using aluminum tape. The flap created an upper surface blockage similar to the effect of the support strut. The resulting symmetrical blockage realigned the upstream flow and eliminated leading edge separation.

A second modification was made to the flat plate as a result of the need to generate a turbulent boundary layer over its surface. This was

done by tripping the flow using Number 70 grit sand. A 0.75 in. strip of double stick tape was applied 0.0625 in. from the leading edge of the flat plate. The sand was sprinkled onto the piece of tape and was then covered with aerosol spray adhesive to ensure it would remain in place during the test runs.

The adjustable diffuser section model was mounted directly on the floor of the wind tunnel test section and actually represented one-half of a diffuser. Therefore, the relevant diffuser throat width parameter used throughout the thesis was H where $W = 2H$. The model was constructed of wood. It was 36 in. long, 8.9 in. wide, and had a varying thickness. From the leading edge to an axial distance of 7 in., the diffuser section thickness had an elliptical shape varying from 0 to 3.75 in. At an axial distance of 7 to 15 in., the model had a constant 3.75 in. thickness. At the 15 in. point from the leading edge, a diverging ramp began. This diverging ramp had a thickness of 3.75 in. at an axial distance of 21 in., declining to a thickness of 0.05 in. at the trailing edge of the diffuser section providing a constant θ of 10 deg. A side view of the diffuser model is shown in Figure 3.

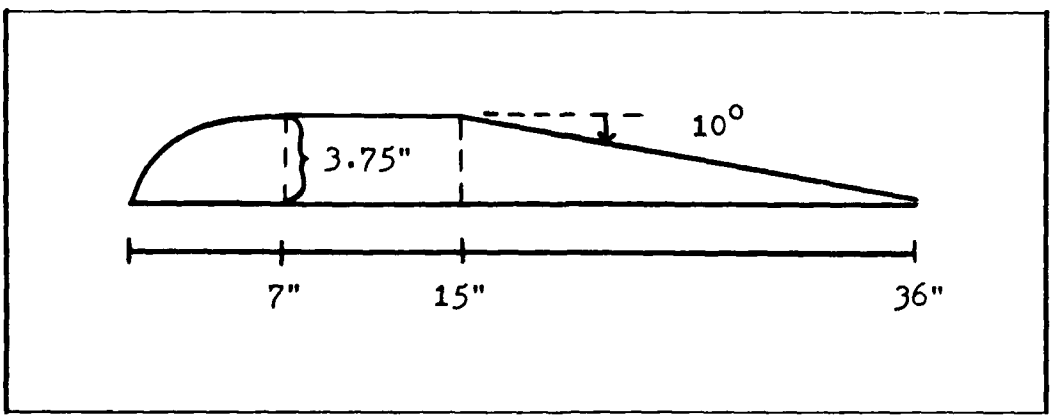

Fig. 3. Side View of the Diffuser Model

A number of flat wood blocks were constructed as supports beneath the diffuser section to raise its height within the tunnel test section (corresponding to a change in H). Each of these blocks was 36 in. long and 8.9 in. wide. The thicknesses of the blocks were 0.125, 0.25, 0.50, 1.0, and 1.5 in. in order to provide a variety of H values. The support blocks and diffuser section were connected together using heavy duty double stick tape.

Initial experimental results indicated that the diffuser model also required modification to eliminate sidewall boundary layer effects. To remedy the inability to generate separated flow, a pair of cardboard vanes were placed within the diffuser, 1.0 in. from each side wall. The vanes extended from the wind tunnel ceiling to the diffuser surface, and along the entire length of the model's diverging channel. The vanes were held in place with strapping tape. A strip of Number 70 grit sand was used to trip the flow in the same manner as was employed for the flat plate model.

During the experiments, flow visualization involving the diffuser section was conducted. The visualization studies were performed by applying oil drops, Dow Corning 200 Fluid, to the plain diffuser surface and observing the resulting pattern created by the flow. Flow visualization of the diffuser surface with and without riblets was conducted with thin tufts of string approximately 1 in. in length. The tufts were attached individually to the riblets using small pieces of strapping tape.

Riblets

Two different types of riblet material were proposed for use in the

wind tunnel experimental research. The first type of riblet material used was Model NPE 266 Scotchcal™ Brand Drag Reduction Tape. The tape is 0.007 in. thick with symmetrical V-shaped grooves having a peak-to-valley height of 0.006 in. The material has an adhesive backing allowing it to be directly applied to the desired surface. The riblet material is manufactured and distributed by the Automotive Systems Division of the 3M Company. However, this material proved not to be suitable for the given flow constraints. This fact is discussed in more detail in the Experimental Procedure section.

The second type of riblet material used in this thesis was machined from a 21 in. long, 8.9 in. wide, and 0.04 in. thick piece of aluminum. Symmetrical V-shaped grooves having a peak-to-valley height and a peak-to-peak width of 0.035 in. were cut into the aluminum sheet. The machined riblets were attached to the diverging ramp of the diffuser section wind tunnel model using heavy duty double stick tape.

Computer Software

Three computer software programs were used during the course of this thesis to process data and prepare the final report. "MathCAD," written by MathSoft, is a mathematics computation program. It was used to automate a number of the mathematical formulas which required solving during the thesis investigation. Data files and data plots were generated using a software package called "Grapher." This software package was written by Golden Software. "Grapher" was also used to create the figures of plotted experimental data included in this report. The thesis transcript was prepared using "Leading Edge Word Processing" written by Leading Edge Software Products. "Leading Edge Word

Processing" was used on a Leading Edge Model D personal computer and the final transcript was printed on an Epson LQ-800 letter quality printer.

IV. Experimental Procedure

The experiments performed in this thesis were basically divided into three groups. The first set was performed in order to calibrate the experimental apparatus. The discussion of this calibration process is contained in Appendix A. The second group of experiments was performed to validate the accuracy of the methods employed in calculating the flow properties required for analysis and comparison. As a result of the second set of experiments, credible methods for identifying turbulent and laminar boundary layers and calculating their respective drag coefficient, C_D, on a surface were established. A complete discussion of the methodology validation procedure and experiments is contained in Appendix B. The last group of experiments involved the study of the effect of riblets on flow separation in the diffuser section described in the Experimental Apparatus section.

Before applying the riblets, it was necessary to determine the location of flow separation on the plain diffuser section. First, the hot film anemometer was used to ensure the presence of turbulent flow. Dow Corning 200 oil drops were applied to the diffuser surface to determine the location of separation. Since oil drops will streak in the direction of any flow present on a surface, they will remain round when they are not being affected by the flow indicating a region of separation. The height of the diffuser was adjusted within the wind tunnel test section by placing different combinations of the blocks underneath the section. Data collection consisted of recording the x-location of flow separation from the leading edge of the expansion region

of the diffuser for a given flow velocity. All separation locations found using the flow visualization method were verified using Stratford's criteria (Equation 6). The velocity input (as part of the Reynolds number term) required to solve Equation 6 was found by using the hot film anemometer. A boundary layer survey was measured at the diffuser throat to ensure the flow entering the expanding channel had a uniform freestream velocity.

The unsuitability of the 0.006 in. riblets was verified experimentally. The verifying experiment was conducted by applying the 3M riblet film to the flat plate used during the methodology validation procedure discussed in Appendix B. The hot film anemometer was used to measure the boundary layer over the flat plate model with riblets and the corresponding C_D was calculated using Equation 21 found in Appendix B. This C_D was the same as the plain flat plate value, thereby verifying that the smaller riblets had no effect on the viscous drag resulting from the flow over the flat plate.

Experimental and theoretical analysis showed that the 0.035 in. machined riblets should be attached to the diffuser section for this investigation. Flow visualization employing thin tufts of string, measuring approximately one inch in length, attached to the grooves was used to determine the diffuser with riblets flow separation locations.

Plain Diffuser Initial Tests

Flow separation in the diffuser section without riblets was investigated first. Before any tests were conducted, it was necessary to ensure the boundary layer on the diffuser surface was turbulent in order to provide a valid comparison between the plain diffuser and the diffuser

with riblets. The hot film anemometer was used to measure the boundary layer velocity profile at the diffuser throat. Comparing the measured boundary layer profile to the verified profile in Appendix B (Figure 22) indicated the flow was turbulent.

Once it was determined the flow was turbulent, initial experiments were conducted to see if separation occurred as shown in Figure 2. This figure shows flow separation in two-dimensional straight-walled diffusers as a function of the diffuser geometry. For the model used in this thesis, 2θ and L were held constant. The diffuser geometry was altered within the wind tunnel by adjusting H. The model was designed to have a L/2H ratio range between 2 and 7 at a 2θ of 20 deg. According to Figure 2, this would allow the flow through the diffuser to transition from the no separation to separation regime by adjusting H. However, initial visualization tests using oil drops showed completely attached flow on the diffuser surface for any combination of H and wind tunnel velocity. In an attempt to generate separation, 2θ was increased, but this also proved unsuccessful.

It was discovered that the inability to produce separation was due to boundary layers forming on each side of the wind tunnel far upstream from the test section. These boundary layers generated vortices in the flow over the model which were strong enough to keep the flow attached to the diffuser surface.

To alleviate the formation of the vortices, a pair of vanes were placed in the diffuser. The vanes acted as "fences," shielding the model from highly vortical wall boundary layers as well as reinitializing the boundary layer on the vane surfaces. The boundary layer forming on the vanes was much smaller than the tunnel wall boundary layers, producing

weaker vortices (if any at all) in the flow over the model and allowing it to separate as predicted.

After installing the vanes, another check of the boundary layer at the diffuser throat showed the flow was laminar. In order to generate a turbulent boundary layer, a flow trip consisting of a strip of Number 70 grit sand was placed on the model 7.5 in. upstream of the diffuser throat. This had the intended effect: the formation of a turbulent boundary layer at the diffuser throat.

Having installed the vanes and verified the flow was turbulent, separation tests were again conducted. The results of these runs showed two-dimensional flow across the width of the diffuser and the existence of steady, two-dimensional stall.

Data Collection Reference Parameters

Recall from the Experimental Apparatus section that two types of riblets were available for use in this thesis. The decision on the size of the riblets, h, to be applied to the diffuser model was based on the available speed range of the tunnel. Theoretically, the slower the flow speed, the larger the size of the boundary layer forming on a surface. Combining the low speed range of the wind tunnel with the necessity to operate it at slower velocities so as not to dislodge the installed vanes, the boundary layer forming on the diffuser surface was found to be relatively large. Recalling that riblets must extend through the laminar sublayer into the transitional region of the turbulent boundary layer in order to be effective in reducing viscous drag, the use of smaller riblets was rejected.

Relevant flow velocities were needed prior to performing tests. In

order to determine these velocities, it was necessary to ensure that a nondimensional riblet height, h^+, between 8 and 30 could be obtained. For this analysis, a relationship between h and the diffuser throat velocity, U_{th}, was needed. It was assumed that the required velocity-h relationship could be inferred from a skin-friction coefficient value obtained from the diffuser wall expansion region. Substituting Equation 4 into Equation 1 and solving for U_{th} resulted in the following relationship:

$$U_{th} = h^+/[h(C_f/2)^{1/2}] \tag{7}$$

where

U_{th} = diffuser throat velocity, $U_{th} = U_e$ (ft/sec)

This relationship will yield the required U_{th}; given a riblet height, h, a prescribed value of h^+, and the calculated value for C_f obtained from rearranging Equation 4 as follows:

$$C_f = 2(U_\tau/U_e)^2 \tag{8}$$

In order to determine U_e and U_τ, a boundary layer survey was taken on the plain diffuser wall, 10.5 in. from the diffuser throat (x = 10.5 in.). This location was selected because it was the midpoint of the diffuser expanding channel section.

The friction velocity was calculated by applying Cole's wake function. This expression "... can be used to predict the mean-velocity distributions in both the inner and outer regions" of the turbulent boundary layer (3:123). Cole's velocity-profile expression is written as follows:

$$u^+ = \phi_1(y^+) + [\Pi(x)/\kappa]\, w(y/\delta) \qquad (9)$$

where

u^+ = dimensionless velocity parameter, $u^+ = U/U_\tau$
U = flow velocity in the boundary layer at y (ft/sec)
$\phi_1(y^+)$ = turbulent boundary layer law-of-the-wall function
$\Pi(x)$ = Cole's profile parameter
κ = von Karman's mixing-length constant
$w(y/\delta)$ = Cole's wake function

If Equation 9 is evaluated at $y = \delta$, $\Pi(x)$ can be eliminated resulting in Equation 10:

$$U/U_\tau = (1/\kappa)\ \ln(yU_\tau/\nu) + c + [U_e/U_\tau - (1/\kappa)\ \ln(yU_\tau/\nu) - c]\ \sin^2[\pi y/(2\delta)] \qquad (10)$$

where

y = local vertical height (ft)
c = Cole's integration constant with a value between 4.9 and 5.5
δ = boundary layer thickness (ft)

There are two unknowns in Equation 10; U_τ and δ. Solving for U_τ can be done by using just two boundary layer values or, more accurately, by minimizing the root-mean-square of all the data errors. All terms in Equation 10 are moved to the right hand side and set equal to an error parameter, ϵ. A value of δ is then guessed, and a range of U_τ is used with diffuser wall boundary layer data, y and U, to produce a corresponding range of ϵ values. Taking the square root of the sum of the squares of ϵ produces a value proportional to the root-mean-square-error (ϵ_{rms}) for the chosen δ. This procedure is performed for a number of different δ's, a graph made of U_τ versus ϵ_{rms}, and the minimum value of each ϵ_{rms}-U_τ curve connected. The minimum value on this new curve represents the U_τ corresponding to the smallest ϵ_{rms}. For the diffuser,

U_τ was calculated to be 2.11 ft/sec. Substituting this value, along with an assumed U_e of 48.81 ft/sec, into Equation 8 resulted in a diffuser wall C_f of 0.003738. This C_f value was assumed to vary little when used as one input into Equation 7.

The value of h^+ used in Equation 7 was based upon the results obtained from previous studies with riblets. As stated in the Theory section, riblets exhibit the ability to reduce viscous drag for h^+ values up to 30, with the maximum drag reduction occurring for values between 8 and 15 (1:168; 15:3; 16:485; 17:134). For the thesis, three h^+ values were selected within this riblet effectiveness range. One additional value greater than 30 was chosen in order to observe if the effectiveness range was altered for riblets attached to a diffuser instead of a flat plate. Having previously selected h to be 0.035 in., Equation 7, with the calculated values for C_f and h^+, provided the U_{th} values at which flow separation data was to be collected. The tunnel idle speed of 19.0 ft/sec caused a lower limit on h^+. Table 1 shows the four chosen h^+ values and the corresponding U_{th} values used for data collection in the thesis.

Table 1. U_{th} and h^+ Values Used for Data Collection

U_{th} (ft/sec)	h^+
19.0	14.5
29.0	21.9
39.0	29.5
51.0	38.1

With the U_{th} values determined, the next data collection parameter

requiring calculation dealt with the diffuser geometry. For the model used in the thesis, the only variable was the throat width, H. To determine the range of H's to be used as data collection reference points, a number of flow separation test runs were made varying H with respect to the U_{th} values shown in Table 1. The results of these runs showed for H less than 1.75 in., inconsistent flow separation locations were obtained. This was probably due to boundary layer interference from the wind tunnel ceiling. For H greater than 4.25 in., completely attached flow on the diffuser surface was observed. Therefore, five H values between 1.75 and 4.25 in. were selected as the reference points for flow separation data collection. These five H values were 1.75, 2.25, 2.75, 3.25, and 4.25 in.

V. Results and Discussion

The experiments were designed to show the effect of riblets on the location of flow separation in a subsonic diffuser. By comparing the data obtained for two cases (plain diffuser and diffuser with riblets), conclusions were made as to the overall effect of riblets upon subsonic diffuser flow separation. Flow separation in the diffuser section without riblets was investigated first.

Plain Diffuser Data

Having completed the initial verification tests and determined the data collection reference parameters, the flow separation locations in the plain diffuser were observed and recorded. Data collection involved setting the diffuser to a given H and recording the flow separation location for each U_{th}. As in previous runs, oil drops were used to visually define the flow separation location. Stratford's method (Equation 6) was used as a numerical comparison to check the visually obtained data. Table 2 shows the diffuser flow separation locations as a function of H and U_{th} determined using both the visualization method and Stratford's method, as well as the percentage difference between the two. Also, a few locations were checked using cotton tufts and Head's method (3:166-167) for further separation location verification. The value of $x_{sep} = 21.00$ appearing in the table refers to the situation where no flow separation was measured, i.e., where the flow was completely attached.

The information in Table 2 shows certain trends. In all cases, Stratford's method predicts a slightly earlier flow separation in the

Table 2. Plain Diffuser Flow Separation Locations (x_{sep})

U_{th} (ft/sec)	H (in.)	x_{sep} (in.) Visualization Method	Stratford's Method	Percent Difference	Head's Method
19.0	1.75	5.00	4.80	4.00	
29.0		* 5.63	5.28	6.22	
39.0		6.13	5.76	6.04	
51.0		6.44	6.12	4.97	
19.0	2.25	* 6.63	6.36	4.07	
29.0		7.06	6.96	1.42	
39.0		8.00	7.80	2.50	
51.0		9.06	8.64	4.64	
19.0	2.75	8.50	8.28	2.59	8.76
29.0		9.44	9.24	2.12	9.68
39.0		10.50	10.32	1.71	10.71
51.0		* 11.44	11.16	2.45	11.64
19.0	3.25	* 10.25	10.20	0.48	
29.0		11.63	11.52	0.95	
39.0		* 12.63	12.60	0.24	
51.0		15.44	15.36	0.52	
19.0	4.25	14.44	14.28	1.11	
29.0		* 16.81	16.44	2.20	
39.0		19.75	19.44	1.57	
51.0		* 21.00	21.00	0.00	

* Cotton tufts were also used to verify these locations.

diffuser than the visualization method indicates. This is a result which also shows up in the data presented by Cebeci and Smith (3:378-384). The percentage difference between the two methods ranges from 0.24% to 6.22%, with an average difference of approximately 2.60%. The larger percentage differences occur for H = 1.75 in. and the smallest at H = 3.25 in. ,

for all U_{th} values. The percentage difference between the visualization and Stratford's methods are well within acceptable limits verifying the separation locations appearing in Table 2.

Diffuser With Riblets Data

The next step in the thesis data collection process was to investigate the flow separation in the diffuser section with riblets applied to its surface. The machined riblets were attached to the surface using heavy duty double stick tape. A small amount of epoxy was applied under the leading edge of the riblets to ensure it was securely attached to the diffuser surface in an attempt to reduce the generation of undesirable flow disturbances. With the riblets in place, diffuser separation location data was collected with respect to the U_{th} and H values previously determined. It was discovered oil drops could not be used to visualize the flow pattern in this case since the grooves or valleys of the riblet surface caused the oil drops to run and streak even before the tunnel flow was turned on. Instead, thin tufts of string were used to visualize the flow pattern over the riblet surface. Six tufts were placed in a row across the width of the diffuser. Small pieces of strapping tape, measuring approximately 0.15 in. square, were used to fasten the base of each tuft to the riblets. The row of tufts was moved up from the diffuser exit until the flow separation location was determined. Only one row of tufts was used in order to minimize the disturbance of the flow over the riblets.

The flow separation locations obtained for the diffuser with riblets are shown in Table 3. Also shown in Table 3 are the results for the plain diffuser to provide a comparison between the two cases. As was the

Table 3. Comparison of the Flow Separation Locations (x_{sep}) for the Diffuser With and Without Riblets

U_{th}	H	x_{sep} (in.)	
(ft/sec)	(in.)	No Riblets	Riblets
19.0	1.75	5.00	16.44
29.0		5.63	19.71
39.0		6.13	20.75
51.0		6.44	21.00
19.0	2.25	6.63	15.44
29.0		7.06	18.40
39.0		8.00	19.98
51.0		9.06	21.00
19.0	2.75	8.50	13.04
29.0		9.44	19.31
39.0		10.50	19.92
51.0		11.44	20.69
19.0	3.25	10.25	16.10
29.0		11.63	19.60
39.0		12.63	20.13
51.0		15.44	21.00
19.0	4.25	14.44	15.25
29.0		16.81	17.77
39.0		19.75	20.65
51.0		21.00	21.00

case in Table 2, x_{sep} = 21.00 in. means the flow was completely attached to the diffuser surface.

The values in Table 3 for the diffuser with riblets case were obtained by averaging the separation locations obtained from three independent test runs for each data collection point. Three runs were made for each data point in order to improve the accuracy of the results. The largest variation between the three separation values

obtained for any particular data collection point was 0.25 in. Since no numerical method exists for predicting flow separation over a riblet surface, no verification of the data could be made as was done for the plain diffuser.

Data Analysis

Dimensional Data Analysis. The first step in the analysis process was to investigate the specific data values obtained from the experimental research. The most important issue this analysis needed to resolve was whether or not the use of riblets could delay flow separation in a subsonic diffuser. Figures 4 through 8 show a comparison of the flow separation locations for the diffuser with and without riblets as a function of U_{th}, for each individual H. For every H, the separation location occurred farther downstream for the diffuser with riblets than it did for the plain diffuser. This result indicates the use of riblets does indeed delay flow separation in a subsonic diffuser as compared to the same configuration not employing riblets. Also, the delay in separation was found to be significant for the smaller H values. The largest difference in separation location between the diffuser with and without riblets (Δx_{sep}) occurred for H = 1.75 in. At this H, the average increase (averaged with respect to the four U_{th} values) in separation location was approximately 236%. The percentage difference decreased as H increased, with the minimum average value (5.3%) occurring for H = 4.25 in.

Figure 9 shows Δx_{sep} as a function of U_{th} for all five experimental H values. For all of the data points except one, as H increased, for a given U_{th}, Δx_{sep} decreased. As stated previously, this relationship

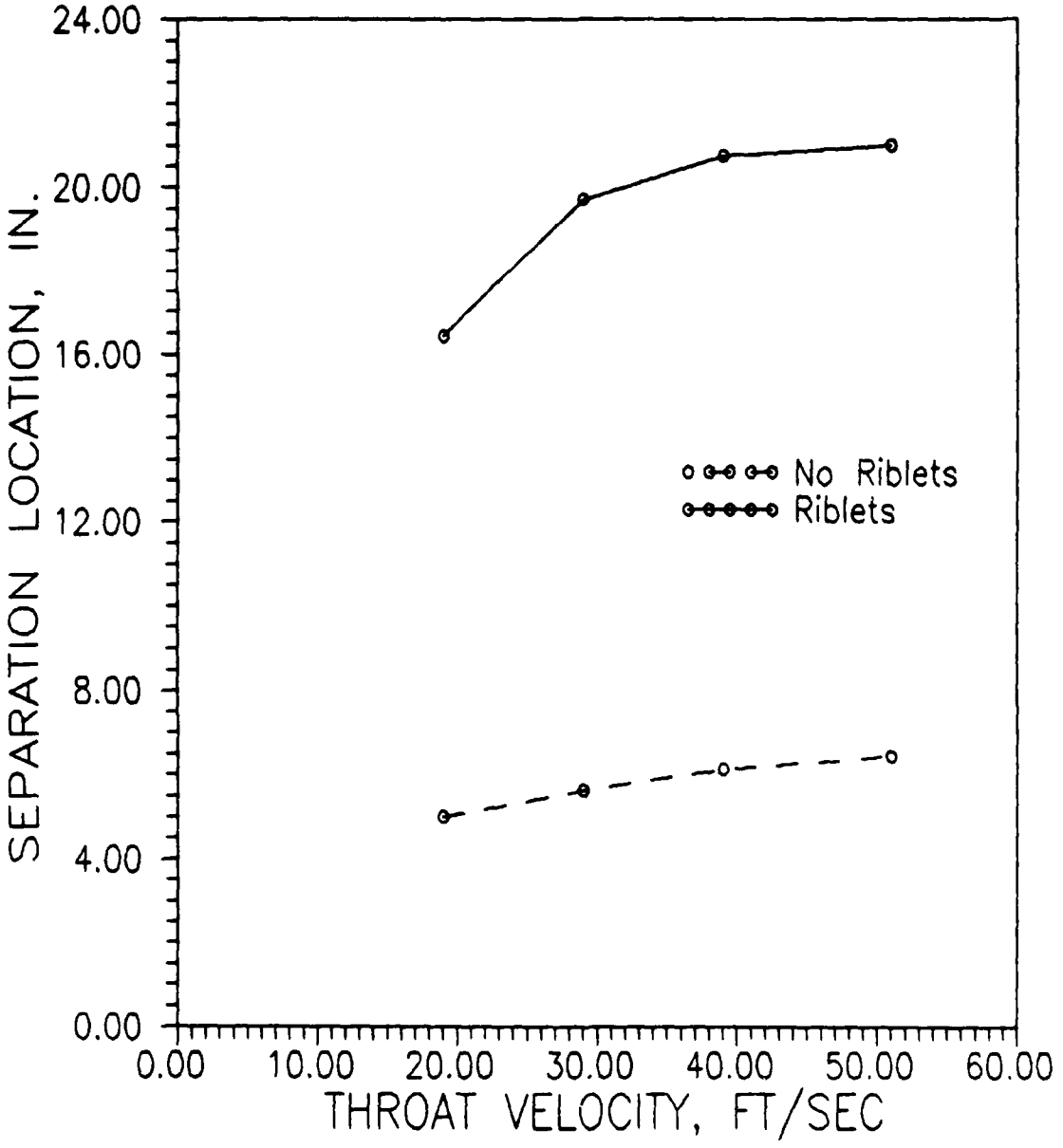

Fig. 4. Throat Velocity Versus Separation Location for Diffuser With and Without Riblets at H = 1.75 in.

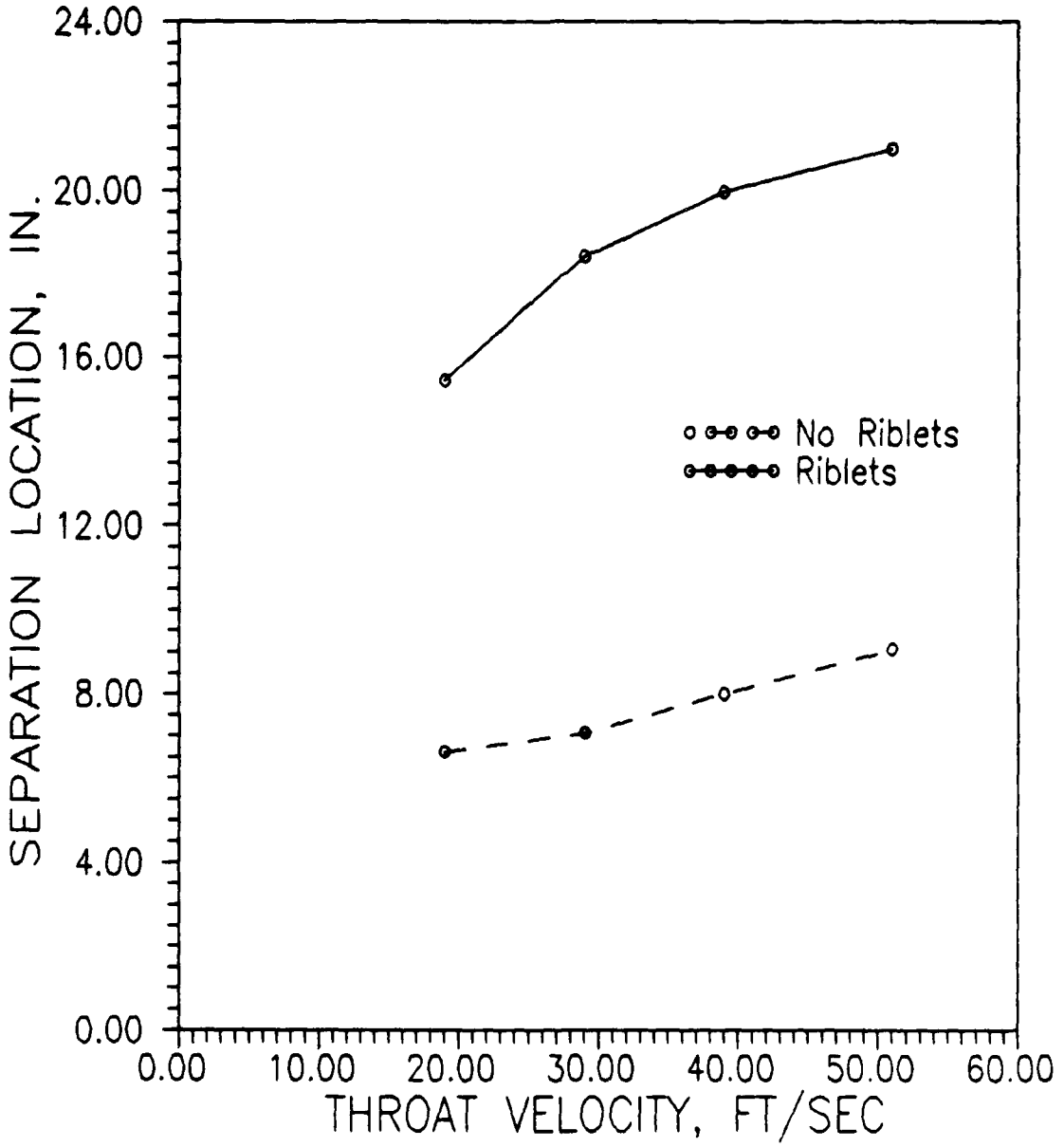

Fig. 5. Throat Velocity Versus Separation Location for Diffuser With and Without Riblets at H = 2.25 in.

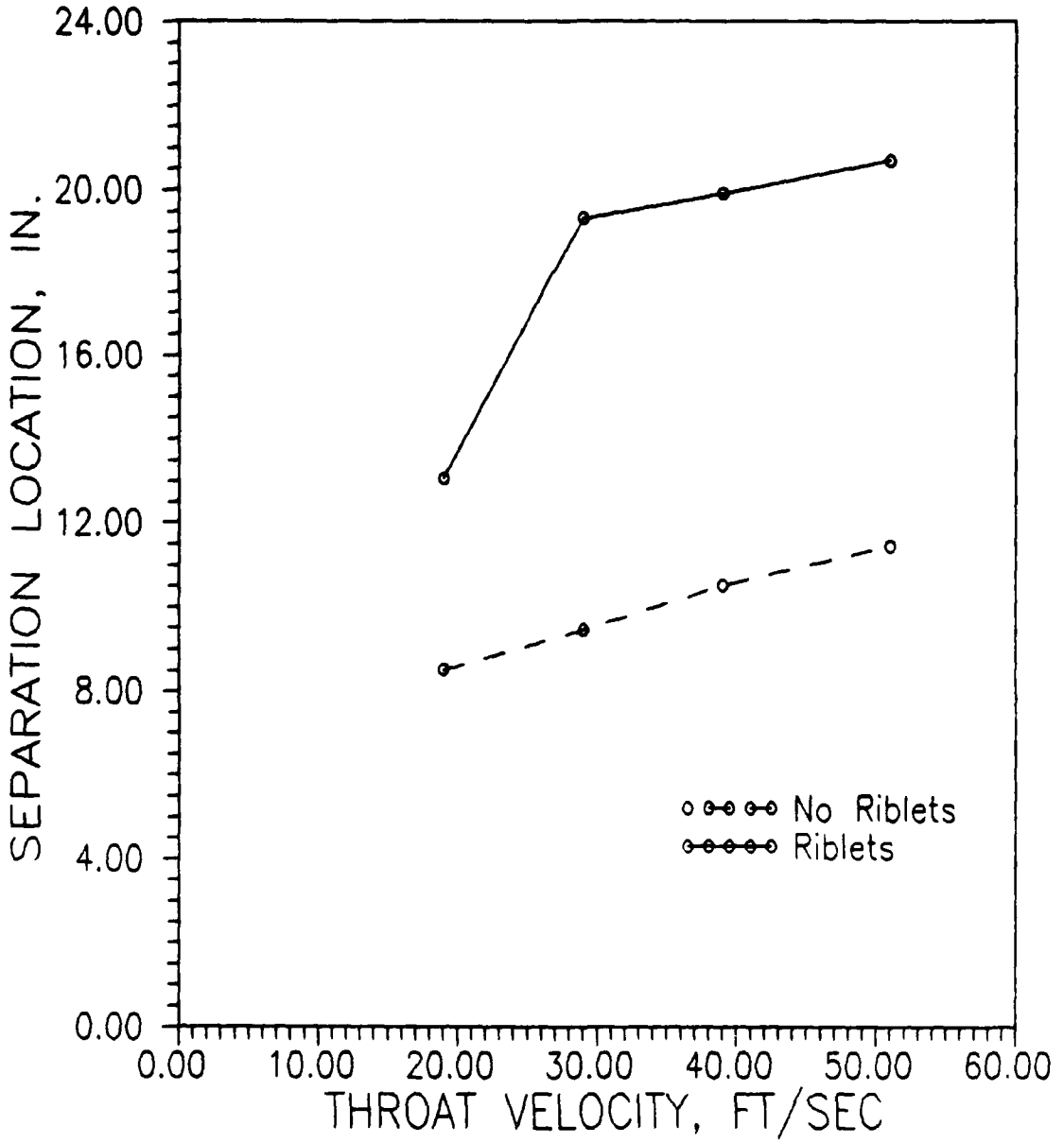

Fig. 6. Throat Velocity Versus Separation Location for Diffuser With and Without Riblets at H = 2.75 in.

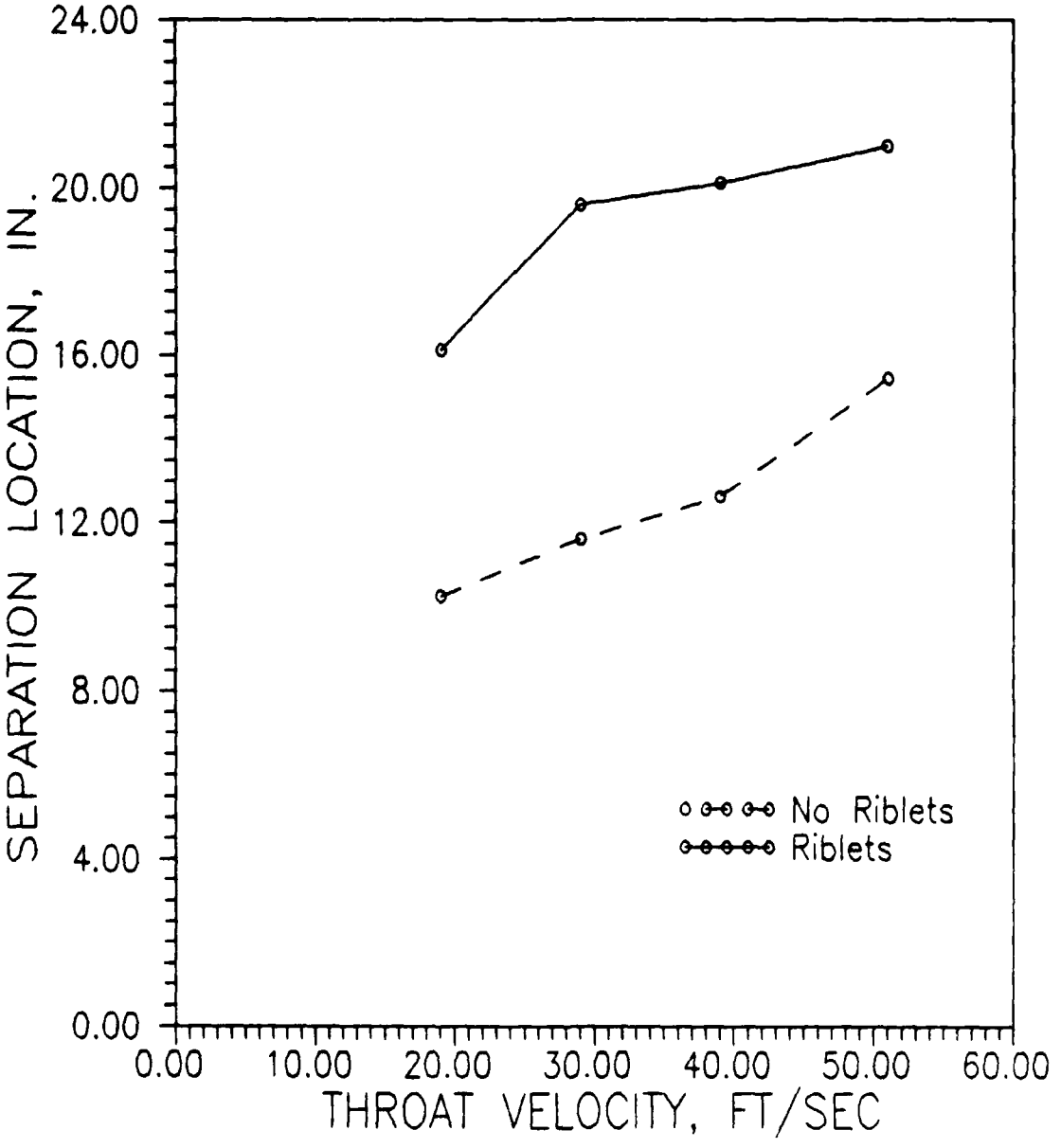

Fig. 7. Throat Velocity Versus Separation Location for Diffuser With and Without Riblets at H = 3.25 in.

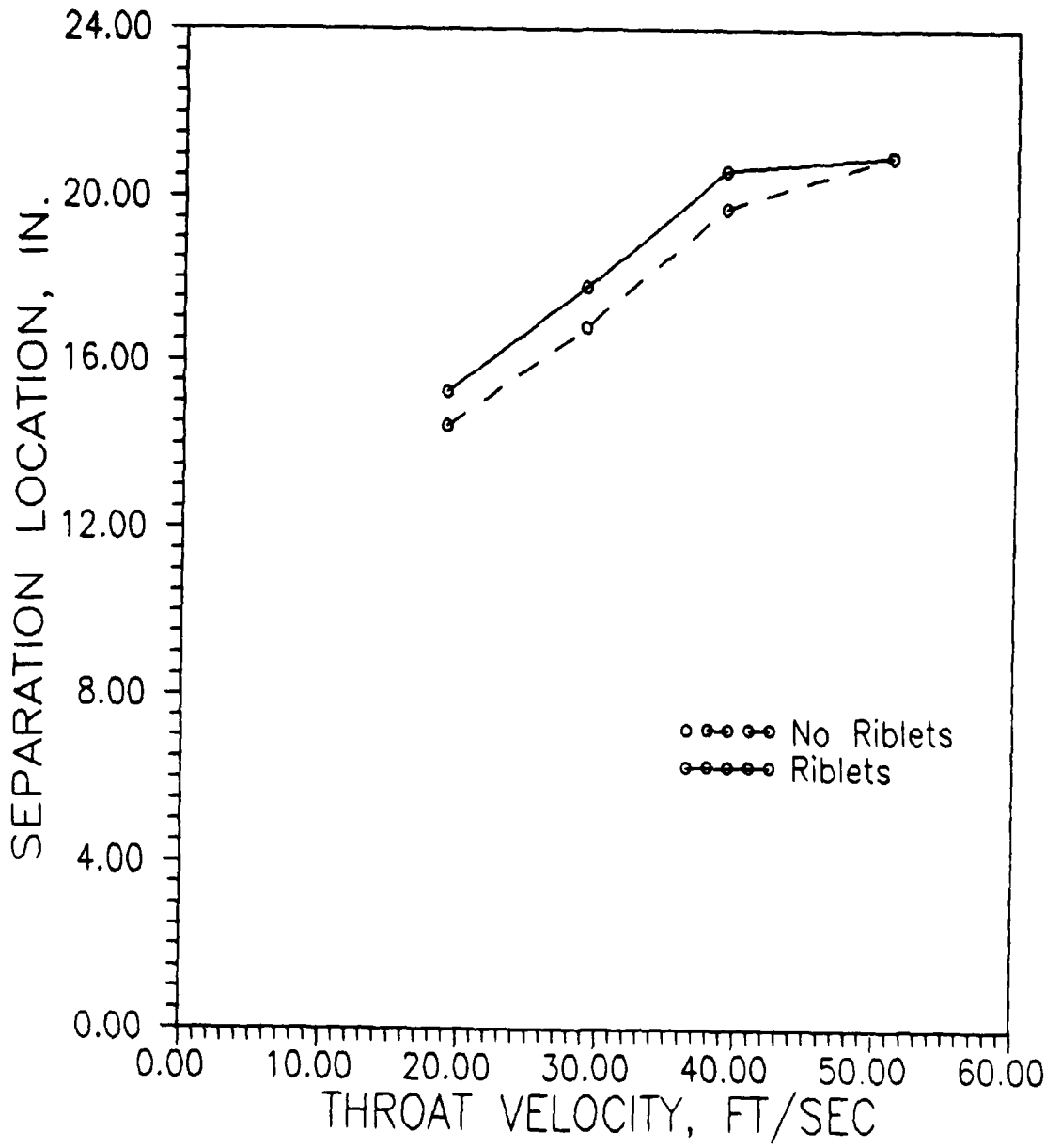

Fig. 8. Throat Velocity Versus Separation Location for Diffuser With and Without Riblets at H = 4.25 in.

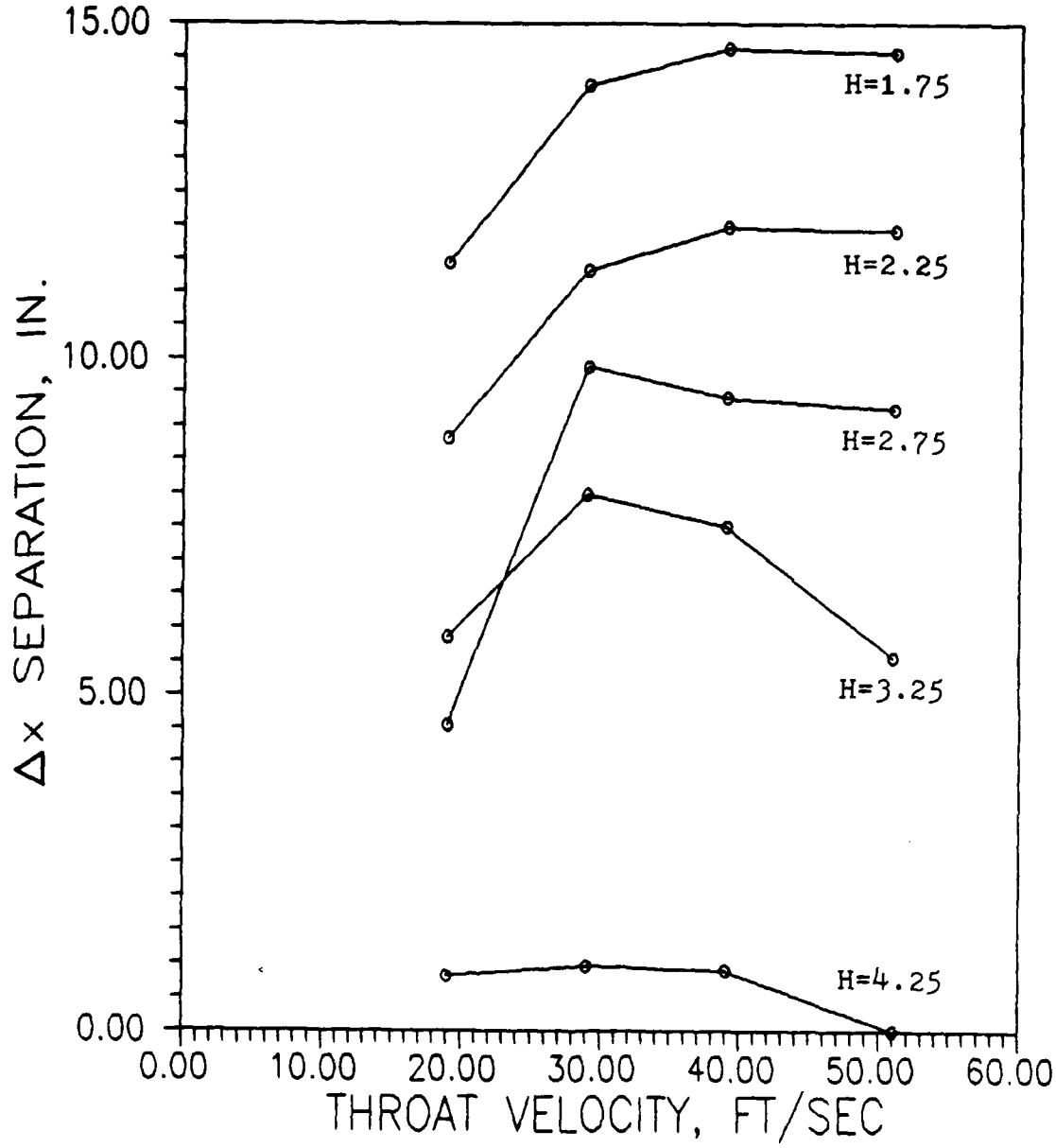

Fig. 9. Throat Velocity Versus Difference in Separation Location Between Diffuser With and Without Riblets for All Throat Widths (H)

indicates riblets have their greatest influence in delaying flow separation at smaller values of H. For H equal to 1.75 and 2.25 in., Figure 9 also shows Δx_{sep} increases between U_{th} of 19.0 and 39.0 ft/sec where it then begins to decrease for all following velocities. For H equal to 2.75, 3.25, and 4.25 in., Δx_{sep} increases between U_{th} of 19.0 and 29.0 ft/sec before it begins to decrease. A review of Table 6 also shows the largest percentage increase in flow separation location occurs at U_{th} = 29.0 ft/sec for every H. From this observation it can be stated riblets have their greatest influence in delaying flow separation at smaller U_{th} values (between 19.0 and 29.0) for any H.

Recalling Table 1, U_{th} corresponds to a specific value of h^+ at the diffuser throat (h^+_{th}). Using Table 1, h^+_{th} was substituted for U_{th} and then compared to Δx_{sep}. Such a process revealed Δx_{sep} increased as h^+_{th} increased from 14.5 to 21.9. For h^+_{th} greater than approximately 22, Δx_{sep} decreased. This trend agrees reasonably well with the results of experiments conducted using riblets applied to a flat plate, previously discussed in the Theory section. These experiments showed the viscous drag reducing capability of riblets was maximized for h^+ between 8 and 15 and still effective up to a value of 30. In the case of the diffuser used in this work, it appears the viscous drag reducing capability of riblets is maximized for h^+_{th} = 22 (corresponding to maximum Δx_{sep}) and then decreases as h^+_{th} increases beyond this value.

Further review of Figures 4 through 8 revealed a number of other characteristics. For both the riblet and no riblet cases, the actual separation location increased, or occurred farther downstream, in the diffuser as U_{th} increased. For the plain diffuser, this increase appeared to be basically linear with velocity. For the riblets, there

seemed to be a greater sensitivity to speed at the lower velocities and less at the higher ones. Also, the difference in the separation locations between the riblet and no riblet cases decreased as H increased. This was due mainly to the plain diffuser flow which tended to stay attached for longer distances with increasing H.

Figure 10 was generated by combining Figures 4 through 8 into one graph. This graph portrays the flow separation locations for the diffuser with and without riblets as a function of U_{th}, for all five H values. The inverse relationship between H and Δx_{sep} is very apparent in Figure 10. Also evident in the figure is the steady increase in actual separation location as H increases for the plain diffuser. However, the separation locations for the diffuser with riblets case basically remain grouped together with the H values actually intermixing. It appears no clear relationship exists for predicting measured separation locations for a subsonic diffuser with riblets. However, a wider range of H values should be investigated to more clearly understand the existence, or nonexistence, of any such relationships.

Another view of the data is presented in Figures 11 through 14. In these figures, a comparison of the riblet and no riblet flow separation locations as a function of H, for each individual U_{th}, is shown. These figures show that flow separation location varies almost linearly with H for the plain diffuser. For the diffuser with riblets, separation location seems to be insensitive to H. This observation agrees with the earlier statement concerning the lack of a trend relating H to the separation location in a diffuser with riblets.

Figure 15 was created by combining Figures 11 through 14 and shows flow separation location versus H for all four U_{th} values. Figure 15

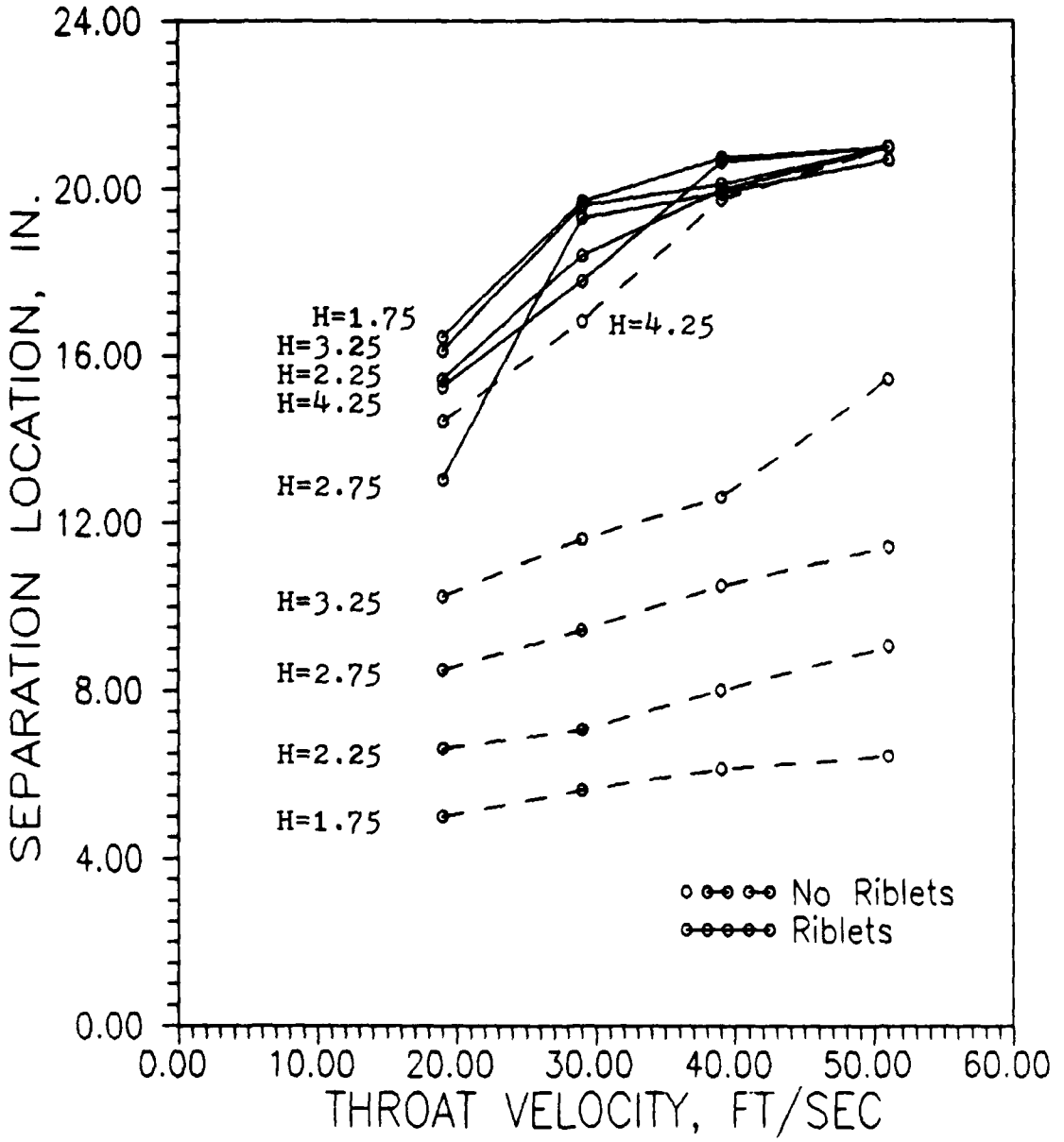

Fig. 10. Throat Velocity Versus Separation Location for Diffuser With and Without Riblets for All Throat Widths (H)

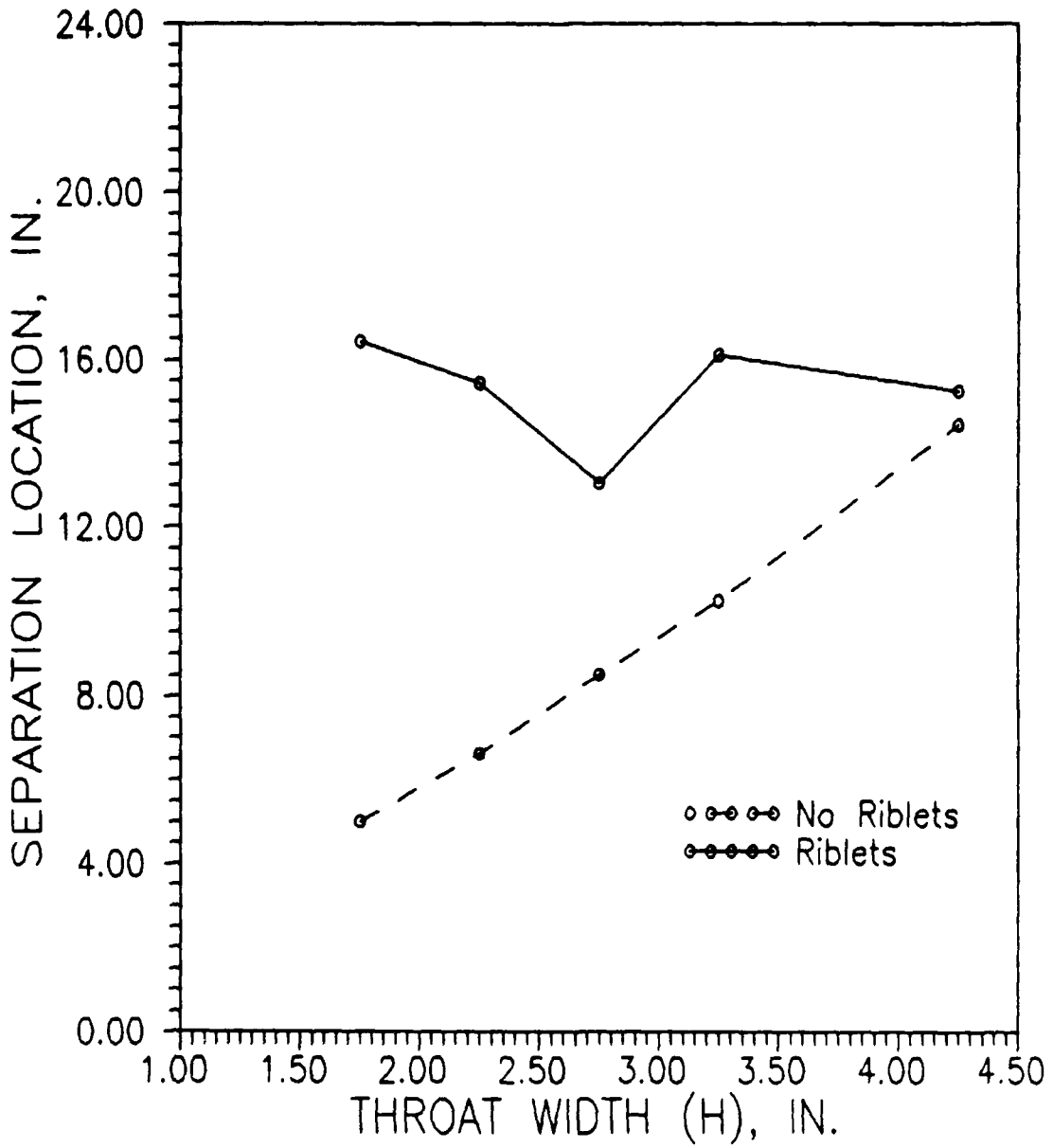

Fig. 11. Throat Width Versus Separation Location for Diffuser With and Without Riblets at V = 19.0 ft/sec

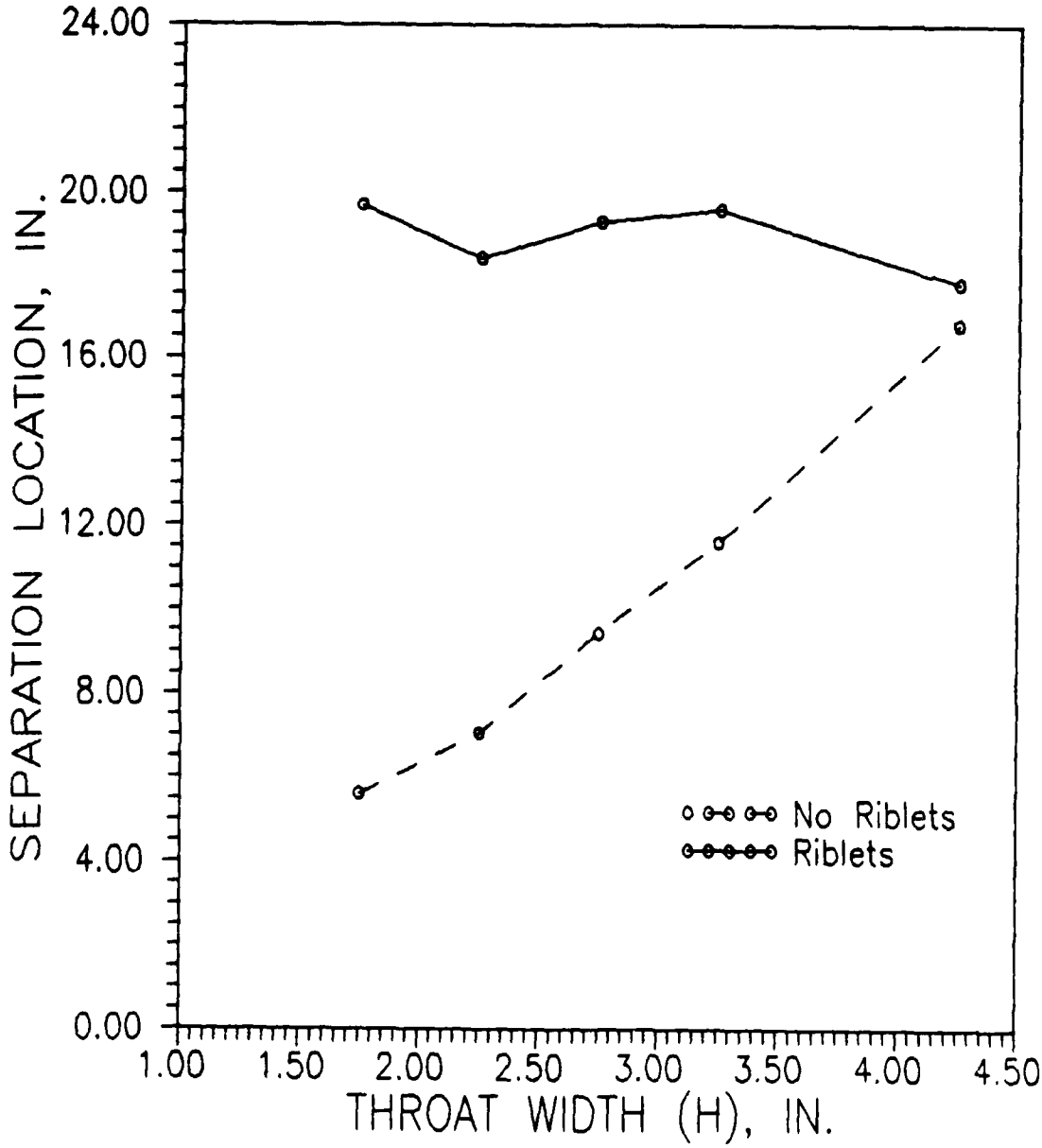

Fig. 12. Throat Width Versus Separation Location for Diffuser With and Without Riblets at V = 29.0 ft/sec

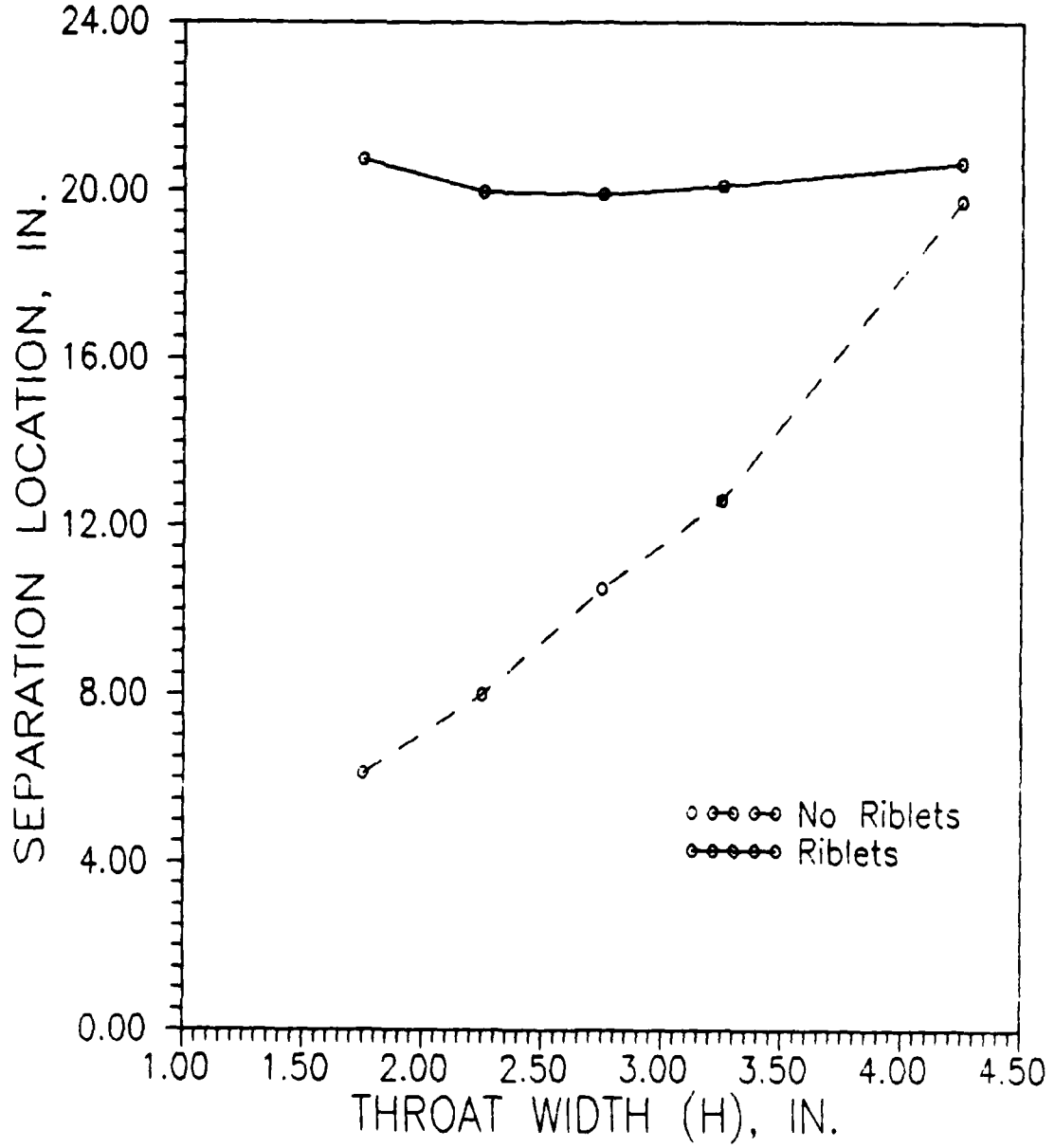

Fig. 13. Throat Width Versus Separation Location for Diffuser With and Without Riblets at V = 39.0 ft/sec

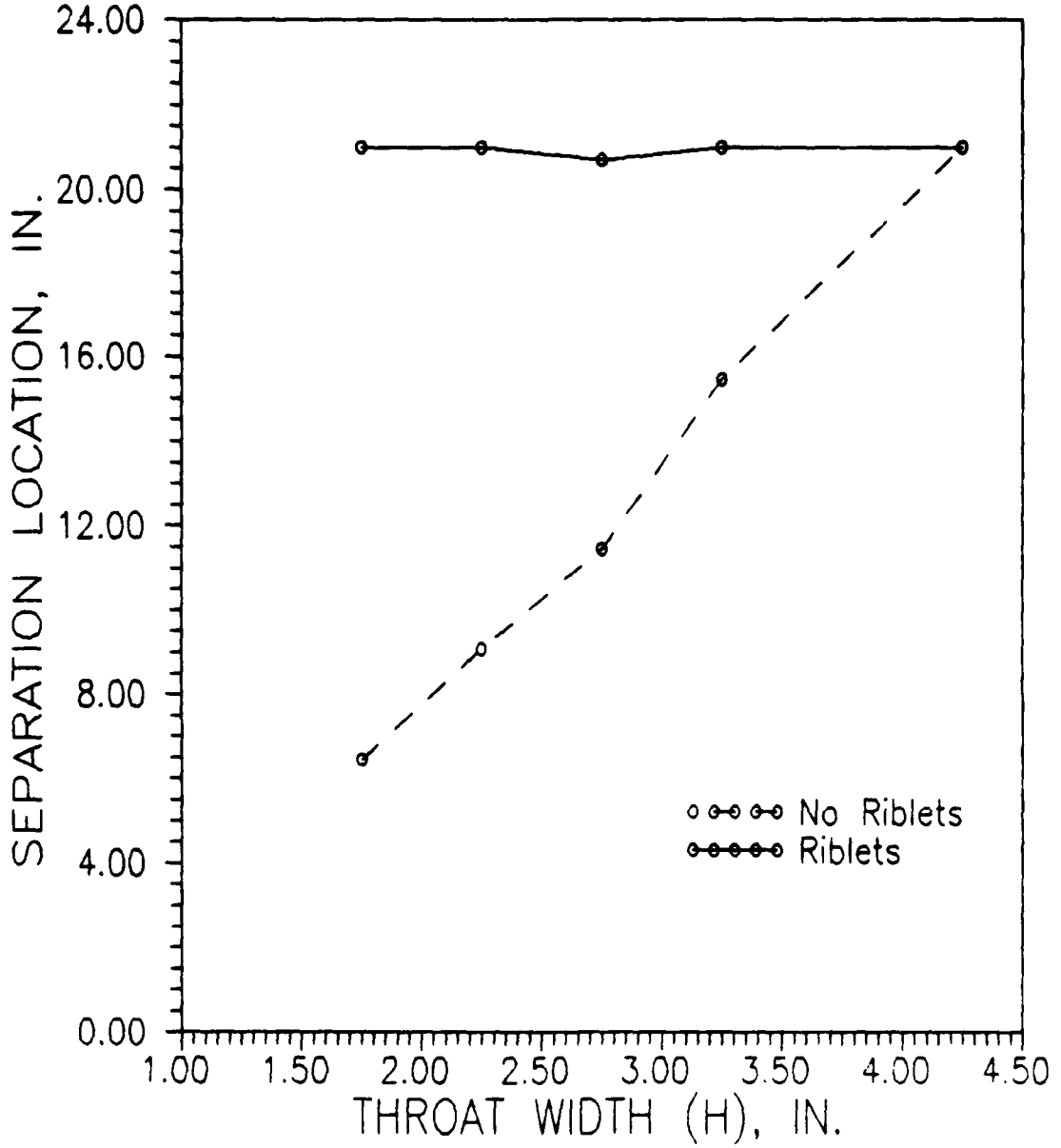

Fig. 14. Throat Width Versus Separation Location for Diffuser With and Without Riblets at V = 51.0 ft/sec

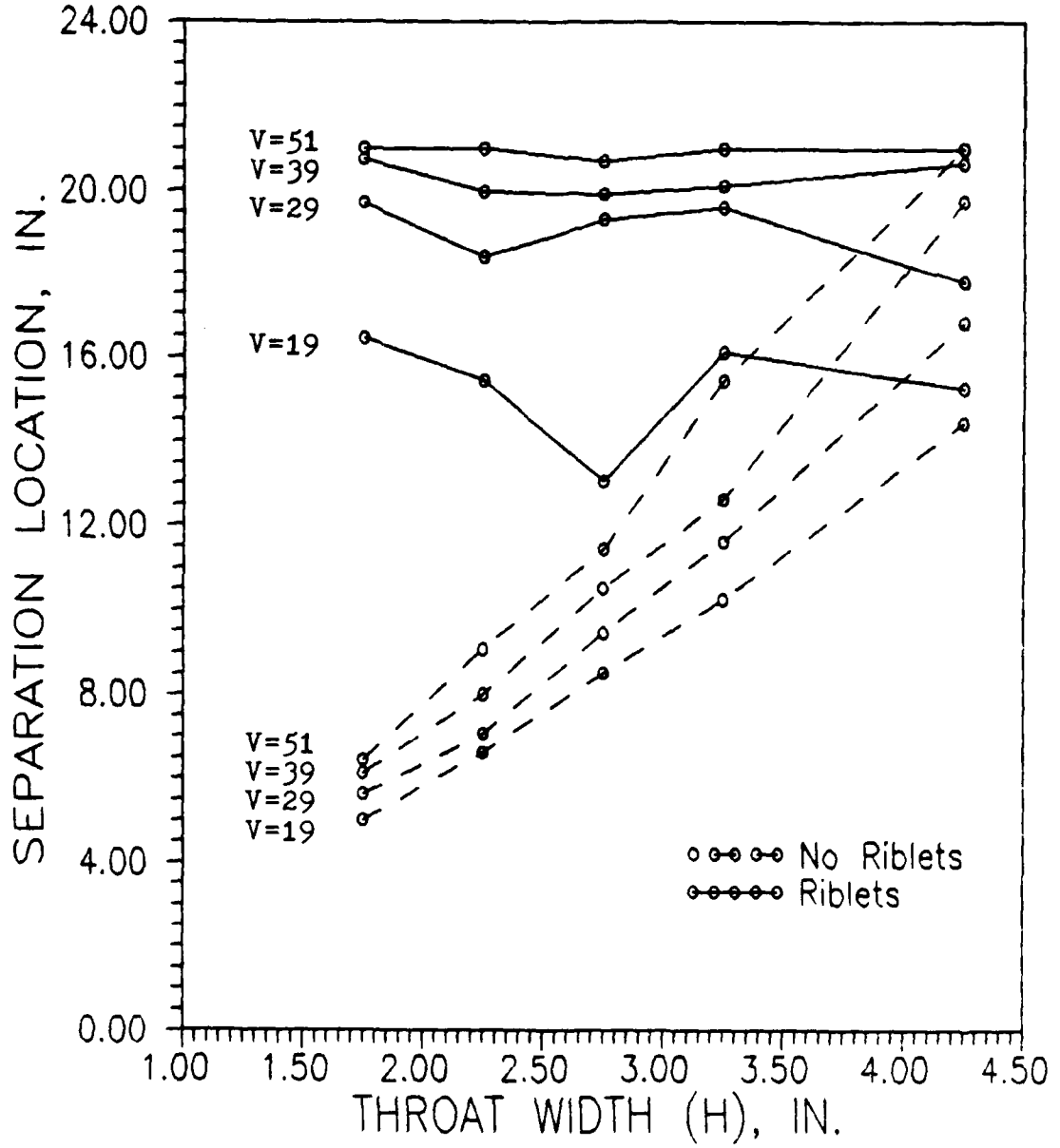

Fig. 15. Throat Width Versus Separation Location for Diffuser With and Without Riblets for All Throat Velocities (V)

clearly shows the increase in flow separation location as U_{th} increases, for a given H, in both the riblets and no riblets cases.

Nondimensional Data Analysis. Nondimensional data analysis was performed in order to determine if any trends existed in the data which could uncouple the results from the specific test setup. By nondimensionalizing the test data, the experimental results could be reviewed and even duplicated independent of the particular procedure and apparatus employed during the thesis. The two dimensionless parameters used in this part of the analysis were the difference in flow separation location between the riblet and no riblet cases divided by the diffuser wall length ($\Delta x_{sep}/L$) and the Reynolds number.

Reynolds number is defined in the following equation:

$$Re = UD_H/\nu \tag{11}$$

where

Re = Reynolds number
U = flow velocity (ft/sec)
D_H = hydraulic diameter (ft)

The velocity parameter, U, represented either U_{th} or the velocity at the diffuser flow separation location (U_{sep}). The continuity equation was used to establish the following relationship for calculating U_{sep} with respect to the geometry of a diffuser:

$$U_{sep} = (HU_{th})/(H + x\sin\theta) \tag{12}$$

where

U_{sep} = velocity at diffuser flow separation location (ft/sec)
H = one half of the diffuser throat width (ft)
x = flow location measured from the minimum pressure point (ft)
θ = one half of the diffuser divergence angle (deg)

The hydraulic diameter, D_H, is a parameter commonly used to eliminate the dependence of geometry in engineering problems. It is also used to normalize the viscous effects of a boundary layer forming on the inside of a duct of arbitrary shape to that of one growing on the interior of a circular duct. The parameter is calculated according to the following equation:

$$D_H = 4A/p \tag{13}$$

where

D_H = hydraulic diameter (ft)
A = duct area (ft^2)
p = duct perimeter (ft)

As it applies to the geometry of a diffuser, D_H is defined according to Equation 14 shown below:

$$D_H = 2w/[1 + w/(H + x\sin\theta)] \tag{14}$$

where

w = diffuser model width (ft)
H = one half of the diffuser throat width (ft)
x = flow location measured from the minimum pressure point (ft)
θ = one half of the diffuser divergence angle (deg)

Recall a pair of vanes were installed in the diffuser used during the thesis. These vanes reduced the effective duct area, or hydraulic diameter, of the wind tunnel. Since each vane was mounted 1.0 in. from the edge of the diffuser model, w was equal to 6.9 in. in Equation 14.

Figure 16 was the first dimensionless graph to be created with the diffuser throat Reynolds number (Re_{th}) being plotted against $\Delta x_{sep}/L$ for all five H values. The Re_{th} was calculated using U_{th} and the diffuser throat D_H. For all of the data points in the figure except one, $\Delta x_{sep}/L$

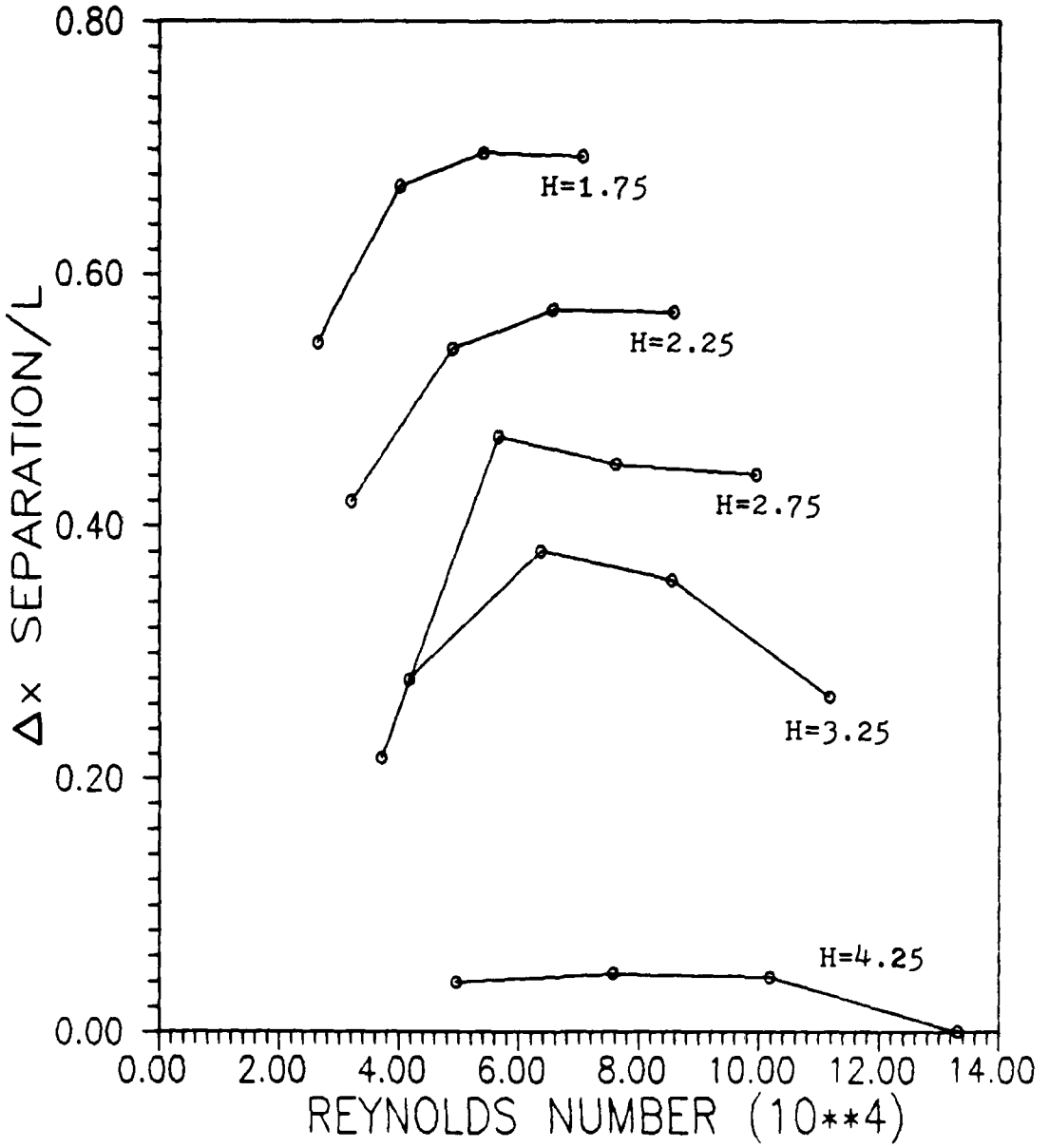

Fig. 16. Throat Velocity/Throat Hydraulic Diameter Reynolds Number Versus Dimensionless Difference in Flow Separation Location for All Throat Widths (H)

decreased as H increased. Also evident in the figure was the fact that for each H, $\Delta x_{sep}/L$ increased until Re_{th} was approximately equal to 63500. For Re_{th} values greater than 63500, $\Delta x_{sep}/L$ began to decrease. This trend indicated riblet effectiveness is dependent upon Re_{th} with an accompanying conclusion that there is a unique riblet size (h) associated with Re_{th} for maximizing the delay in diffuser flow separation. For the riblets used in this thesis (h = 0.035 in.), the most significant delay in flow separation, basically regardless of H, occurred for Re_{th} approximately equal to 63500. Also, Figure 16 is very similar to Figure 9 in appearance.

Figure 17 shows a plot of the flow separation Reynolds number (Re_{sep}), calculated using U_{sep} and the separation location D_H, versus $\Delta x_{sep}/L$ for the five values of H. This figure also shows the well documented trend of a decrease in $\Delta x_{sep}/L$ as H increases. As in Figure 16, the maximum $\Delta x_{sep}/L$ occurred at basically the same Reynolds number for all five H values indicating the existence of a relationship between riblet effectiveness and Re_{sep}. The maximum $\Delta x_{sep}/L$ occurred for Re_{sep} approximately equal to 47500.

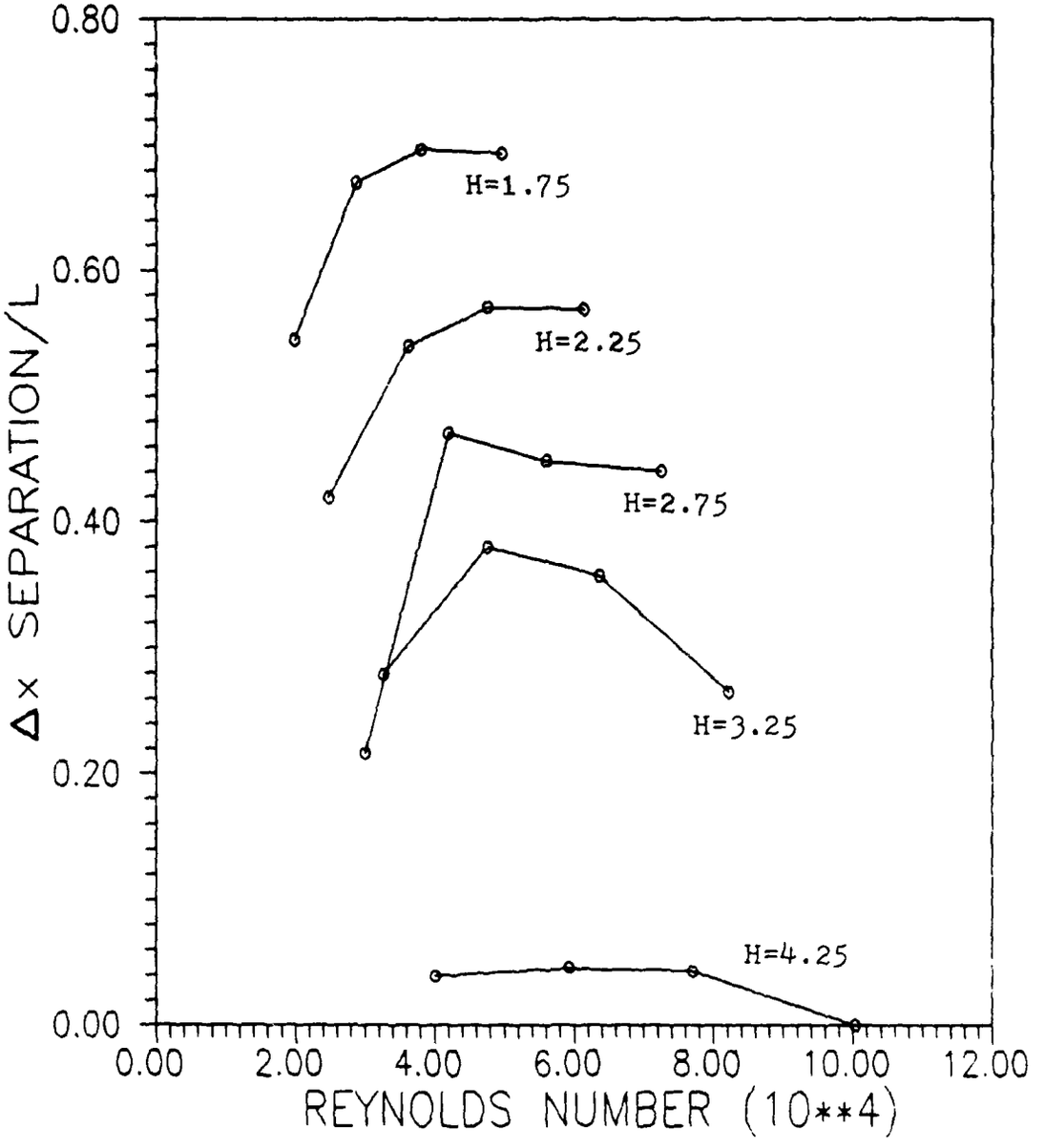

Fig. 17. Separation Velocity/Separation Hydraulic Diameter Reynolds Number Versus Dimensionless Difference in Flow Separation Location for All Throat Widths (H)

VI. Conclusions and Recommendations

Conclusions

As a result of this thesis investigation into the effect of riblets upon flow separation in a two-dimensional straight-walled subsonic diffuser, the following conclusions are made:

1. Most importantly, as it pertains to the specific objective of this thesis, flow separation is delayed in a diffuser employing riblets as compared to a geometrically identical plain diffuser. This result indicates the viscous drag reducing capability of riblets does affect the location of flow separation agreeing with Polzin's experiments which showed that a reduction in diffuser surface roughness delayed the onset of flow separation in a subsonic two-dimensional diffuser (5:161). By using riblets, this effect was shown to be significant with increases in the flow separation location as high as 250% under certain experimental conditions (H = 1.75 in.). This large difference becomes even more significant when one recalls riblets only reduce viscous drag by a maximum amount of 8% (according to previously quoted theory). It is quite interesting to see such a small viscous drag reduction be transformed into such a large flow separation delay in a two-dimensional straight-walled subsonic diffuser. Further study is of course required; however, the initial results shown in this thesis indicate riblets can be used to delay the occurrence of steady, two-dimensional stall, and the accompanying large decrease in pressure recovery and efficiency associated with this flow condition, in a subsonic diffuser.

2. One evident trend in the data is the increase in Δx_{sep} as H

decreases. However, it appears, for a given U_{th}, the measured separation locations for the diffuser employing riblets are basically constant regardless of H. This implies the flow separation is essentially independent of H for the diffuser with riblets in dramatic contrast to plain diffuser theory.

3. An obvious dependence of flow separation upon U_{th} exists for the diffuser employing riblets. As U_{th} increases, so does the measured separation location. A different trend is observed when comparing U_{th} to Δx_{sep}. Initially, as U_{th} increases, Δx_{sep} increases. However, beyond a velocity of 29.0 ft/sec, Δx_{sep} decreases with increasing U_{th}. Therefore, for the riblets used in this thesis (h = 0.035 in.) the greatest Δx_{sep} occurs when U_{th} is approximately equal to 29.0 ft/sec. Substituting h^+_{th} for U_{th}, the maximum Δx_{sep} occurs when $h^+_{th} = 22$. This result for a subsonic diffuser differs slightly from the established theory for flow over a flat plate which states the maximum riblet effectiveness (or the largest decrease in viscous drag) occurs for h^+ between 8 and 15.

4. Analysis of the experimental data also reveals a relationship exists between Reynolds number and $\Delta x_{sep}/L$. For the riblets used in this thesis, the maximum $\Delta x_{sep}/L$ occurs for Re_{th} approximately equal to 63500 and and a Re_{sep} of 47500, independent of the value of H. This indicates there is a unique Reynolds number associated with the maximum effectiveness for a particular riblet geometry.

Recommendations

This thesis revealed a benefit in using riblets for the purpose of delaying flow separation in two-dimensional straight-walled subsonic diffusers. Therefore, further investigation in this area seems

warranted. In regards to future experimental research involving the application of riblets in a subsonic diffuser, the following suggestions are made:

1. The effect of riblets on flow separation needs to be investigated in a complete diffuser as a follow-on to the half diffuser section employed in this thesis. This would allow the complete formation of steady, two-dimensional stall in the diffuser. Such stall is characterized by the generation of fully developed stall on one diffuser wall while the flow over the other surface is relatively smooth and continuous. Also, the influence of riblets upon flow separation with respect to the other two diffuser geometry parameters, L and 2θ, should be explored. The effect of riblets upon flow separation location was researched only as a function of W in this thesis.

2. It is recommended a water table be used to investigate the flow through the diffuser. By using a water table, the diffuser model could be placed so as to eliminate wall interference effects like those experienced in this work. Also, the flow through the diffuser would be easier to visualize using water instead of air, and dye could be injected into the fluid stream to enhance the visualization even more.

3. The effect of riblets on diffuser flow separation needs to be researched at higher subsonic speeds than those investigated in this thesis in order to simulate aircraft flight conditions. By operating at higher velocities, the smaller, commercially available 3M riblets could be used as well. These riblets are much easier to attach to a surface and their use would eliminate the cutting errors or inconsistencies associated with machined riblets.

4. Future data collection should include a measurement of C_f on the

riblet surface in order to quantify the viscous drag reduction experienced on the diffuser wall. Hopefully, this would lead to the development of a relationship between viscous drag reduction and the increase in flow separation location. Due to the inability to measure C_f on the riblet surface in this thesis, no relationship was formulated between h^+ and flow separation location (although a trend between Δx_{sep} and throat h^+ was discussed and quantified). Such a relationship needs to be found in the same way h^+ was related to maximum viscous drag reduction, or riblet effectiveness, for flow over a flat plate in previous research efforts.

Bibliography

1. Walsh, Michael J. "Drag Characteristics of V-Groove and Transverse Curvature Riblets," Viscous Flow Drag Reduction. Progress in Astronautics and Aeronautics, Volume 72, edited by Gary R. Hough. Technical paper from Symposium on Viscous Drag Reduction, Dallas TX, November 1979. 168-184. New York: American Institute of Aeronautics and Astronautics, 1980.

2. Hinze, J. O. Turbulence (Second Edition). New York: McGraw-Hill Book Company, 1975.

3. Cebeci, Tuncer and A. M. O. Smith. Analysis of Turbulent Boundary Layers. Orlando: Academic Press, 1974.

4. Hefner, Jerry N. "Dragging Down Fuel Costs," Aerospace America, 26: 14-16 (January 1988).

5. Chang, Paul K. Separation of Flow. Elmsford NY: Pergamon Press, 1970.

6. Karamcheti, Krishnamurty. Principles of Ideal-Fluid Aerodynamics (Reprint Edition). Malabar FL: Robert E. Krieger Publishing Company, 1980.

7. Hill, Philip G. and Carl R. Peterson. Mechanics and Thermodynamics of Propulsion. Reading MA: Addison-Wesley Publishing Company, 1965.

8. Mattingly, Jack D. and others. Aircraft Engine Design. New York: American Institute of Aeronautics and Astronautics, 1987.

9. Anders, John B. and others. "The Fix for Tough Spots," Aerospace America, 26: 24-27 (January 1988).

10. Walsh, M. J. "Turbulent Boundary Layer Drag Reduction Using Riblets," Proceedings of the AIAA 20th Aerospace Sciences Meeting. Paper No. 82-0169. New York: American Institute of Aeronautics and Astronautics, 1982.

11. Reidy, L. W. and G. W. Anderson. "Drag Reduction for External and Internal Boundary Layers Using Riblets and Polymers," Proceedings of the AIAA 26th Aerospace Sciences Meeting. Paper No. 88-0138. New York: American Institute of Aeronautics and Astronautics, 1988.

12. Hooshmand, D. and others. "An Experimental Study of Changes in the Structure of a Turbulent Boundary Layer Due to Surface Geometry Changes," Proceedings of the AIAA 21st Aerospace Sciences Meeting. Paper No. 83-0230. New York: American Institute of Aeronautics and Astronautics, 1983.

13. Bacher, E. V. and C. R. Smith. "Turbulent Boundary-Layer Modification by Surface Riblets," AIAA Journal, 24-8: 1382-1385 (August 1986).

14. Bacher, E. V. and C. R. Smith. "A Combined Visualization-Anemometry Study of the Turbulent Drag Reducing Mechanisms of Triangular Micro-Groove Surface Modifications," Proceedings of the AIAA Shear Flow Control Conference. Paper No. 85-0548. New York: American Institute of Aeronautics and Astronautics, 1985.

15. Walsh, M. J. and A. M. Lindemann. "Optimization and Application of Riblets for Turbulent Drag Reduction," Proceedings of the AIAA 22nd Aerospace Sciences Meeting. Paper No. 84-0347. New York: American Institute of Aeronautics and Astronautics, 1984.

16. Walsh, Michael J. "Riblets as a Viscous Drag Reduction Technique," AIAA Journal, 21-4: 485-486 (April 1983).

17. Wallace, J. M. and J. L. Balint. "Viscous Drag Reduction Using Streamwise Aligned Riblets: Survey and New Results," Proceedings of the Turbulence Management and Relaminarisation IUTAM Symposium, edited by H. W. Liepmann and R. Narasimha. 133-147. Heidelberg West Germany: Springer-Verlag, 1988.

18. Bower, William W. "An Analytical Procedure for the Calculation of Attached and Separated Subsonic Diffuser Flows," Proceedings of the AIAA/SAE 10th Propulsion Conference. Paper No. 74-1173. New York: American Institute of Aeronautics and Astronautics, 1974.

19. Kline, S. J. "On the Nature of Stall," Transactions of the ASME, Series D: Journal of Basic Engineering, 81-3: 305-320 (September 1959).

20. Reneau, L. R. and others. "Performance and Design of Straight, Two-Dimensional Diffusers," Transactions of the ASME: Journal of Basic Engineering. 141-150 (March 1967).

21. Moore, Carl A. and Stephen J. Kline. Some Effects of Vanes and of Turbulence in Two-Dimensional Wide-Angle Subsonic Diffusers. NACA Technical Note 4080. Washington: National Advisory Committee for Aeronautics, June 1958.

22. Kline, S. J. "Optimum Design of Straight-Walled Diffusers," Transactions of the ASME, Series D: Journal of Basic Engineering, 81-3: 321-331 (September 1959).

23. IFA 100 System Intelligent Flow Analyzer Instruction Manual (Revision C). Thermo-Systems Incorporated, St. Paul MN, August 1987.

24. Operating Instructions and Parts List: Dwyer Inclined and Vertical Portable Manometers. Bulletin D-2. Dwyer Instruments, Inc., Michigan City IN, 1962.

25. King, Paul I. Personal Communication. School of Engineering, Air Force Institute of Technology (AU), Wright-Patterson AFB OH, 15 July 1988.

26. White, Frank M. Viscous Fluid Flow. New York: McGraw-Hill Book Company, 1974.

27. Haven, Capt Brenda. Investigation of Boundary Layer Disturbances Caused by Periodic Heating of a Thin Ribbon. MS thesis, AFIT/GAE/AA/88M-2. School of Engineering, Air Force Institute of Technology (AU), Wright-Patterson AFB OH, March 1988.

Appendix A: Equipment Calibration Procedure

The first group of experiments conducted during this investigation involved the calibration of the experimental apparatus, specifically the hot film anemometer equipment. Basically, the calibration process involves relating bridge voltage to flow velocity. The bridge voltage is provided by the hot film anemometer and correlates to a specific value of flow velocity over a surface or body in the wind tunnel.

Anemometer Assembly

Before the hot film anemometry system could be calibrated, it needed to be assembled. Detailed instructions for the assembly of the hot film anemometer equipment are provided in the IFA 100 System Instruction Manual (23:1-1 to 3-5). Basically, the system was constructed by connecting the IFA 100 to the hot film probe holder. The probe holder was clamped to the manual traversing mechanism described in the Experimental Apparatus section. The hot film boundary layer probe was then inserted into the probe holder, which extended down into the tunnel test section, completing the anemometry system circuit.

Once the hot film anemometer equipment was connected, the IFA 100 System operating parameters needed to be set. There are three sets of parameters which must be calculated and input into the IFA 100 before anemometer readings can be made. These three sets of operating parameters correspond to the IFA 100 System transducer, frequency response, and signal conditioner. The formulation and input of all of the operating parameters is covered in detail in the IFA 100 System Instruction Manual (23:3-5 to 3-16), with a brief discussion to follow.

The transducer parameters consist of cable resistance (23:3-5 to 3-9) and hot film probe operating resistance (23:3-10,3-11). Once the cable resistance is calculated and input into the IFA 100, it will be automatically subtracted from all subsequent hot film probe readings. The operating resistance value is unique for each probe and can be found on the sensor's shipping container label (23:4-5). The frequency response operating parameters must be visually adjusted. This is done by connecting an oscilloscope to the IFA 100 and applying a square wave test signal (located internally to the IFA 100) to the bridge of the hot film anemometer circuit. The frequency response operating parameters consist of bridge and cable compensation (23:3-11 to 3-13). As viewed on the oscilloscope, these parameters are adjusted to produce the proper square wave test signal shape (23:Appendix 1), resulting in the optimization of the IFA 100 System frequency response. The last set of inputs requiring formulation are the signal conditioner operating parameters consisting of offset, gain, and filter (23:3-14 to 3-17,4-18 to 4-20). These parameters adjust the IFA 100 output signal to the specific conditions under which the experimentation is to be conducted. When all of the operating parameters have been input, the IFA 100 is set to the run mode and the anemometer is ready to output bridge voltage data.

Tunnel Velocity

As stated earlier, the hot film anemometer calibration process consists of correlating the IFA 100 System bridge voltage output to flow velocity. At the outset of the experimentation, it was decided to perform the anemometer calibration in the wind tunnel test section. This was done in order to calibrate the boundary layer probes in an

environment, in terms of temperature, barometric pressure, and geometry, duplicating the actual experimental conditions. It was felt this procedure would reduce the error of the experimental data as compared to an external calibration process where differences in the actual test conditions could adversely affect the results of the investigation. Therefore, it was necessary to establish the procedure for calculating the flow velocity in the wind tunnel test section before calibrating the anemometry system. As stated in the Experimental Apparatus section, a manometer, digital thermometer, and barometer were used to provide readings which were substituted into the following equation for wind tunnel velocity:

$$U = 18.27\ [MT/(1.325P)]^{1/2} \qquad (15)$$

where

U = flow velocity (ft/sec)
M = manometer reading (in. of water)
T = absolute temperature (deg Fahrenheit + 460)
P = barometric pressure (in. of mercury)

The constants appearing in the equation, 18.27 and 1.325, represent conversion factors for the perfect gas constant and the specific gravity of mercury, respectively. Equation 15 was provided by Dwyer Instruments, the manufacturer of the water manometer used throughout the experimentation (24:2).

Calibration Procedure

The hot film anemometers used during the experimental research were calibrated using the methods for measuring bridge voltage and flow velocity just discussed. For a hot film anemometer circuit, bridge voltage is related to flow velocity by the following equation (25:5):

$$E^2 = A + B(U^{1/2}) + CU \qquad (16)$$

where

E = bridge voltage (volts)
U = flow velocity (ft/sec)
A,B,C = anemometer constants

The anemometer constants depend upon the flow fluid (water or air) and the sensor being used (23:4-1). These constants are a function of the flow viscosity, thermal conductivity, and Prandtl number (23:4-1). The correlation between bridge voltage and flow velocity can be established for a particular boundary layer probe by determining the value of the anemometer constants in Equation 16.

The first step in calibrating the desired boundary layer probes was to position a sensor in the middle of the wind tunnel test section. The IFA 100 and wind tunnel were then turned on. Calibration data collection consisted of recording the anemometer bride voltage corresponding to a specific velocity as the tunnel speed was adjusted from its minimum to its maximum value. From this data, a graph of $U^{1/2}$ versus E^2 was constructed. The anemometer constants were determined by applying a least squares fit to the graphed curve.

The anemometer constants are sensitive to changes in flow temperature. Due to building air conditioning problems throughout the course of the experimentation, the room temperature in which the wind tunnel was located was subject to change. Instead of calculating a correction factor for temperature, calibration data was collected for the various temperatures the room stabilized at during the investigation period. The three flow temperatures most frequently encountered were 68F, 75F, and 81F. Calibration curves for these three temperatures, for

one of the boundary layer probes used throughout the experimentation, are shown in Figures 18, 19, and 20. Table 4 shows the values of the anemometer constants obtained from the three calibration curves.

Table 4. Anemometer Constants

Temperature (F)	A	B	C
68F	0.453	0.573	-0.012
75F	0.490	0.551	-0.011
81F	0.339	0.593	-0.014

In its present form, Equation 16 does not have much use in the experimental procedure of this research effort. A more applicable form of the equation results from making flow velocity the dependent variable:

$$U = \{-[(1/C)\ (E^2 - A + 0.25B^2/C)]^{1/2} - B/(2C)\}^2 \qquad (17)$$

This equation allows the velocity to be calculated anywhere within the flow regime from the bridge voltage readings output by the anemometer. Basically, the thesis experimental procedure consisted of using a hot film anemometer to probe the flow around a body and converting the sensor's bridge voltage readings to flow velocity values by applying Equation 17. This velocity data was then analyzed to determine the characteristics and behavior of the flow over the surface being investigated.

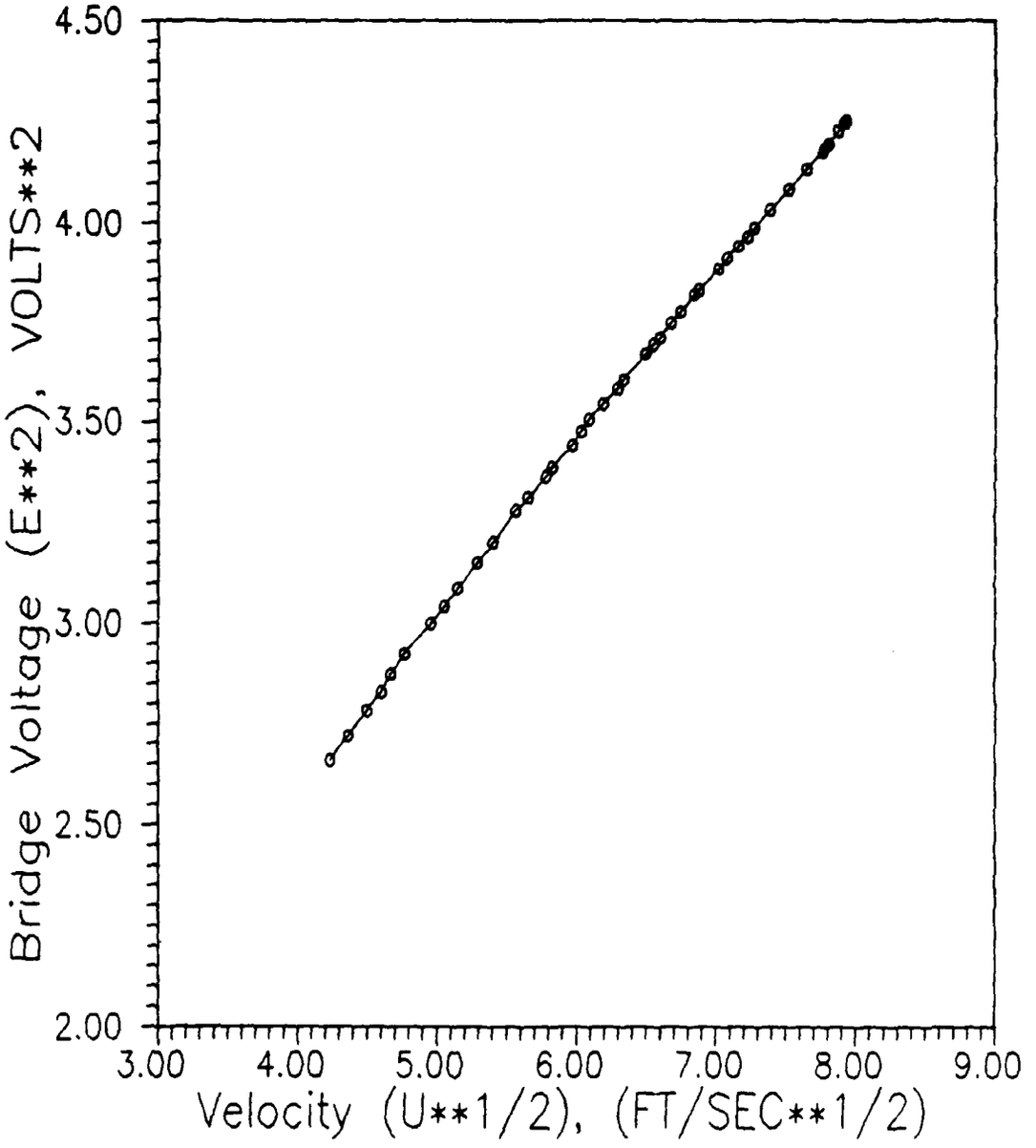

Fig. 18. Anemometer Calibration Curve for 68F

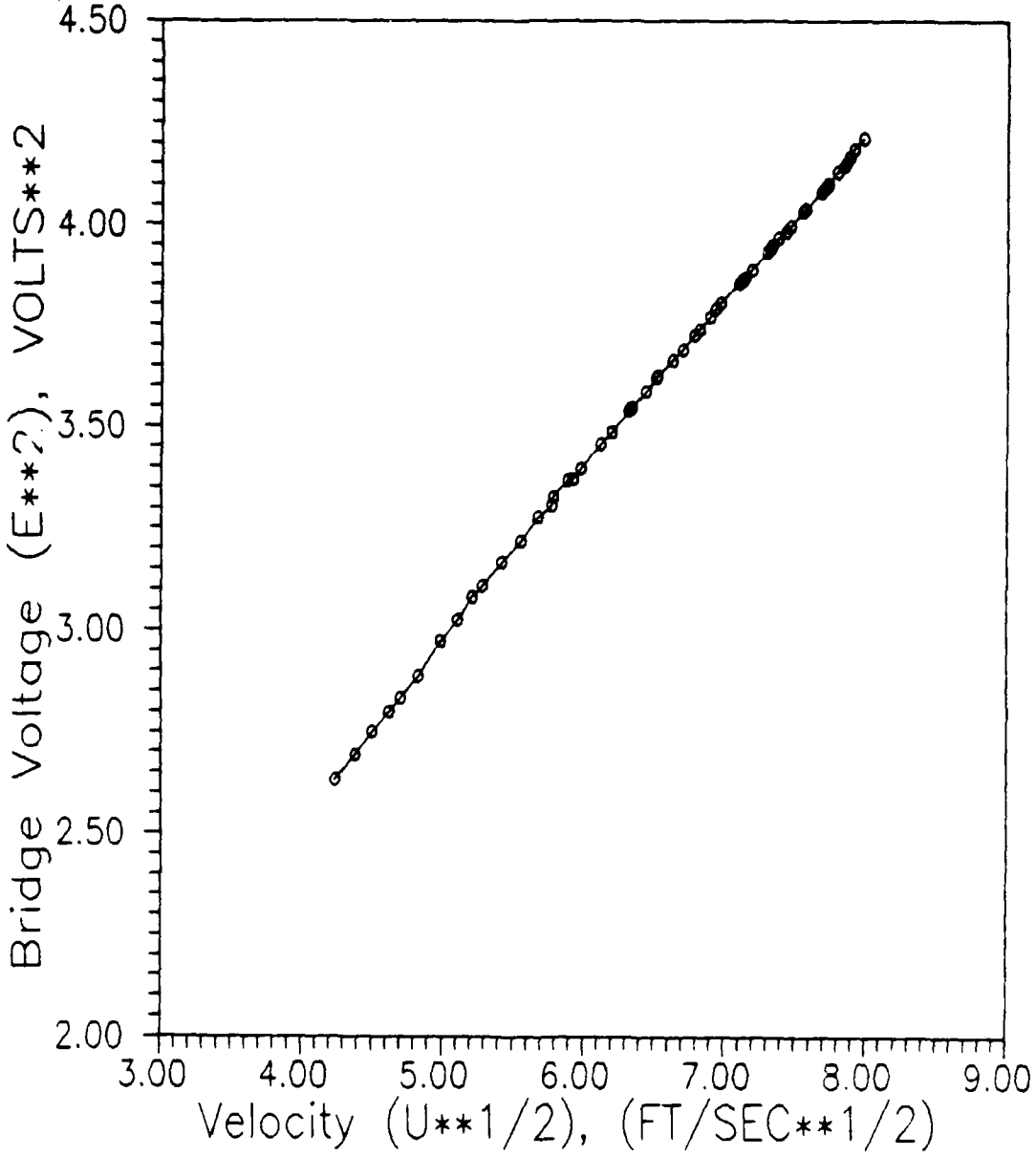

Fig. 19. Anemometer Calibration Curve for 75F

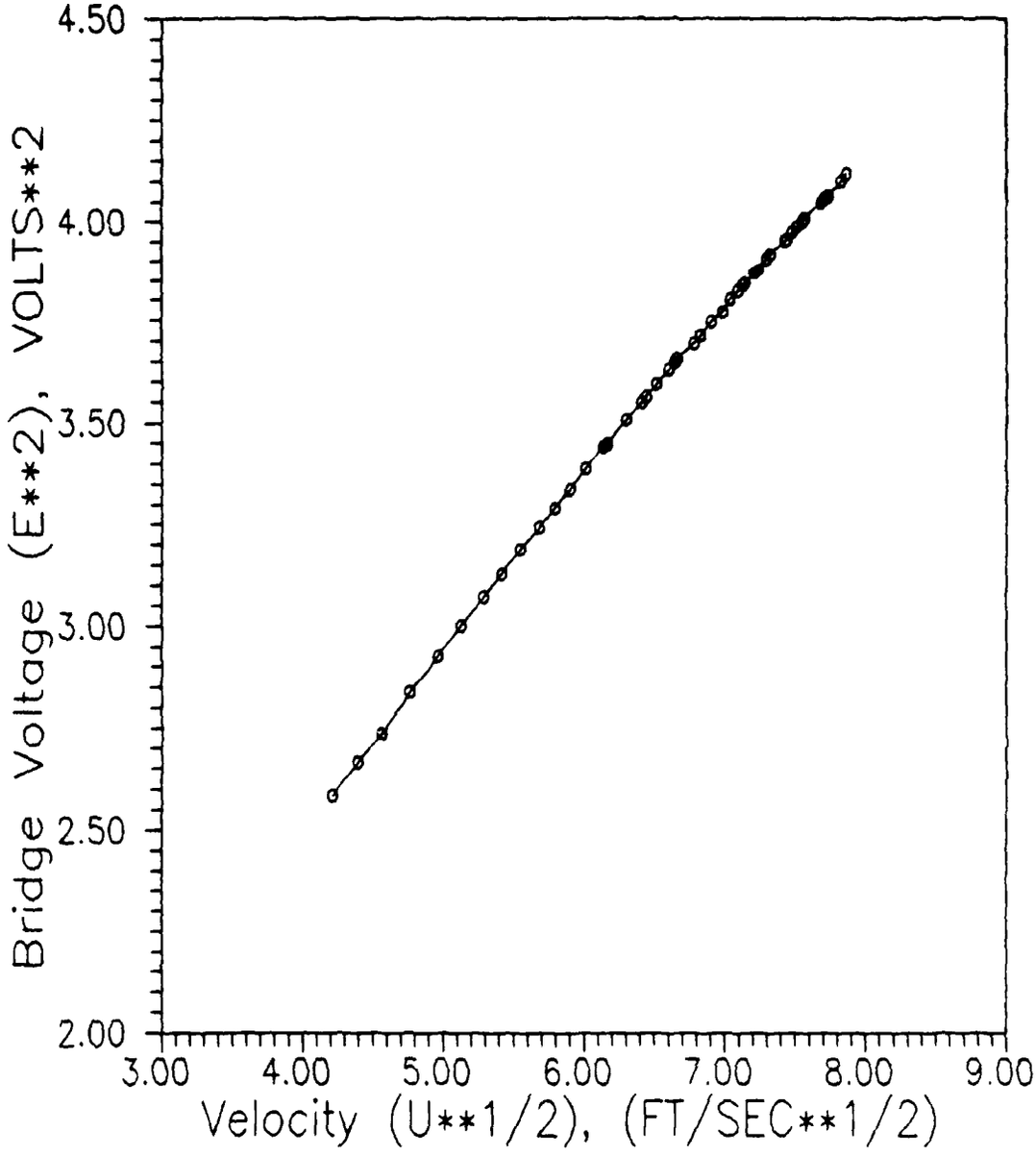

Fig. 20. Anemometer Calibration Curve for 81F

Appendix B: Methodology Validation Procedure

The second set of thesis experiments were performed in order to validate the experimental apparatus and accompanying methodology in analyzing various flow characteristics. This involved evaluating the ability of the hot film anemometer equipment to experimentally determine the flow type (laminar or turbulent) and its corresponding C_D on a surface. The surface used for the methodology validation process was the flat plate model described in the Experimental Apparatus section. The accuracy of the experimentally generated data was determined by comparing it with results obtained from well established theoretical and numerical methods.

Laminar Flow

Laminar flow was the first type of flow studied. The Blasius solution for a laminar boundary layer on a flat plate was used as the exact answer. The Blasius solution can be graphically portrayed by plotting u/U versus η, where u is the local flow velocity, U is the freestream velocity, and η is defined as follows (26:262):

$$\eta = y[U/(2\nu x)]^{1/2} \tag{18}$$

where

ν = kinematic viscosity (ft^2/sec)
η = Blasius solution flow constant
y = local vertical height (ft)
U = freestream velocity (ft/sec)
x = horizontal location along the surface (flat plate) (ft)

The hot film anemometer was used to obtain the necessary data to generate a graph of u/U versus η which was then compared to the Blasius solution.

The experiment was conducted by placing the flat plate model in the wind tunnel and setting the freestream flow velocity to approximately 25 ft/sec. A slower tunnel speed was selected because it generated a larger boundary layer over the surface which was easier to measure with the hot film anemometer. For a given x-location on the flat plate, data collection consisted of obtaining the velocity corresponding to a particular y-location above the surface. Using this data and Equation 18, a plot of u/U versus η was generated.

The first attempt to obtain laminar flow was unsuccessful. It was determined that blockage produced by the asymmetrical model stand was interrupting the flow over the surface. In an attempt to alleviate this problem, the support stand was moved farther back from the plate leading edge. This modification did not correct the flow blockage problem. Research from a previous study in this area indicated the flow blockage interference could be eliminated by attaching an inclined flap to the back end of the flat plate (27:26). The flap supposedly would adjust the oncoming streamlines to the flat plate by balancing the blockage generated by the lower support stand. Haven (27:26) defined the effect of the flap as follows:

> Deflecting the flap upward was equivalent to putting the plate at a negative angle of attack. This enhanced the boundary layer stability by creating a slightly favorable pressure gradient near the leading edge and by eliminating the formation of a stagnation bubble on the upper surface of the model.

After attaching the flap described in the Experimental Apparatus section, laminar flow was obtained over the flat plate. Figure 21 shows a comparison of the experimentally obtained data with the Blasius solution. The experimental data was collected at a flat plate x-location of 3 in. with a freestream velocity of 21.168 ft/sec.

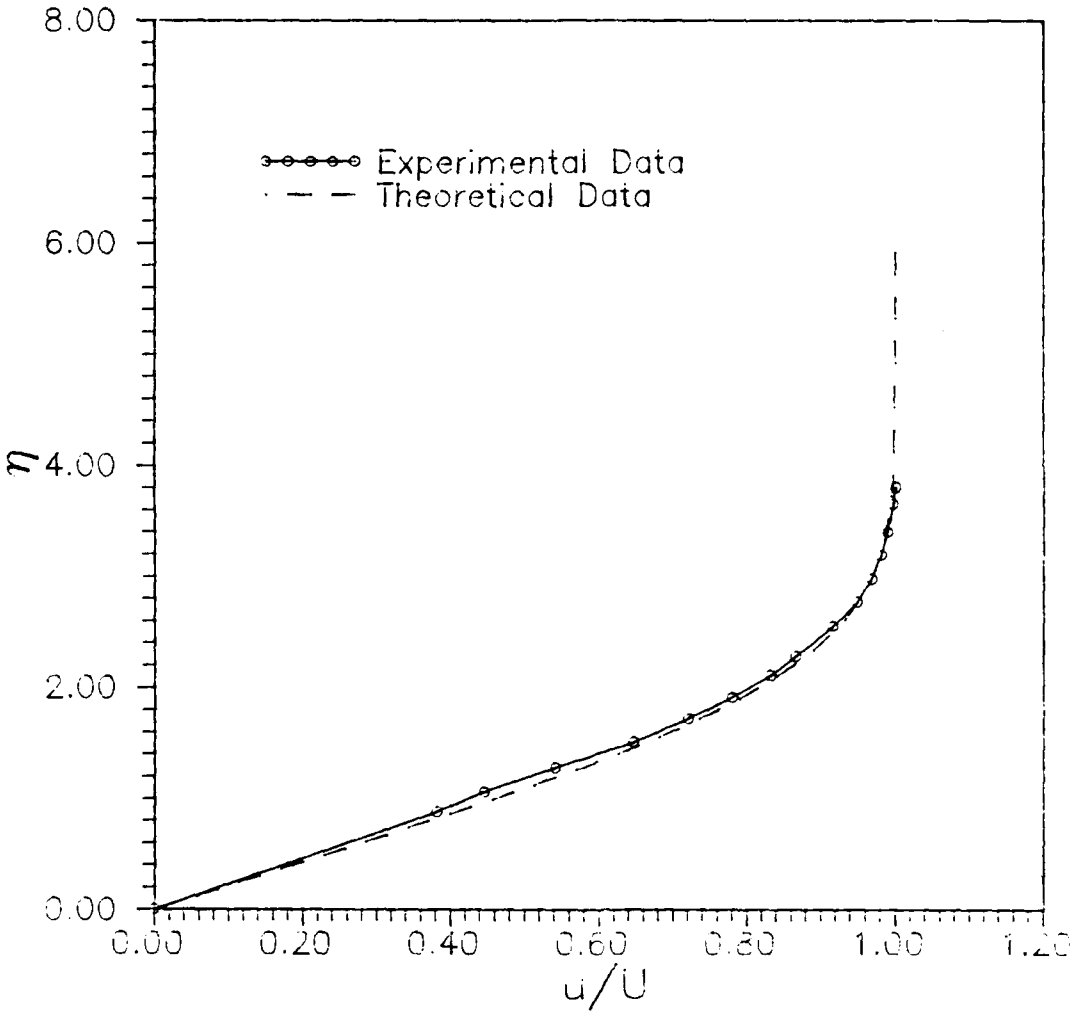

Fig. 21. Experimental and Theoretical Laminar Flow Values for X = 3 in. and U = 21.168 ft/sec
(Theoretical Values from 26:265)

Turbulent Flow

With the ability to experimentally determine laminar flow established, turbulent flow was studied next. The turbulent flow study employed the same experimental procedure as was used for the laminar flow evaluation. However, in order to generate a turbulent boundary on the flat plate, a device was needed to trip the existing laminar flow. The first attempt at tripping the flow involved placing a wire along the leading edge of the flat plate. After several runs using wires of different diameters, this method proved unsuccessful. Instead, a strip of Number 70 Grit sand placed along the plate leading edge was tried. This method provided the necessary conditions to trip the flow and produce a turbulent boundary layer on the flat plate surface. Figure 22 shows the difference in the experimentally obtained turbulent boundary layer to the Blasius laminar boundary layer solution. Also shown in Figure 22 is the 1/7 Power Law ($u/U = (y/\delta)^{1/7}$) solution for a turbulent boundary layer on a flat plate. There is good agreement between the experimental and 1/7 Power Law solutions providing further confirmation of the existence of a turbulent boundary layer on the flat plate surface. The turbulent flow data was collected at a flat plate x-location of 11 in. with a freestream velocity of 50.375 ft/sec.

Drag Coefficient

The last step in the methodology evaluation phase of the thesis was to validate a method to experimentally determine C_D on a surface resulting from a laminar or turbulent boundary layer. Using the momentum approach presented by White (26:243-244), the drag over a surface can be calculated as follows:

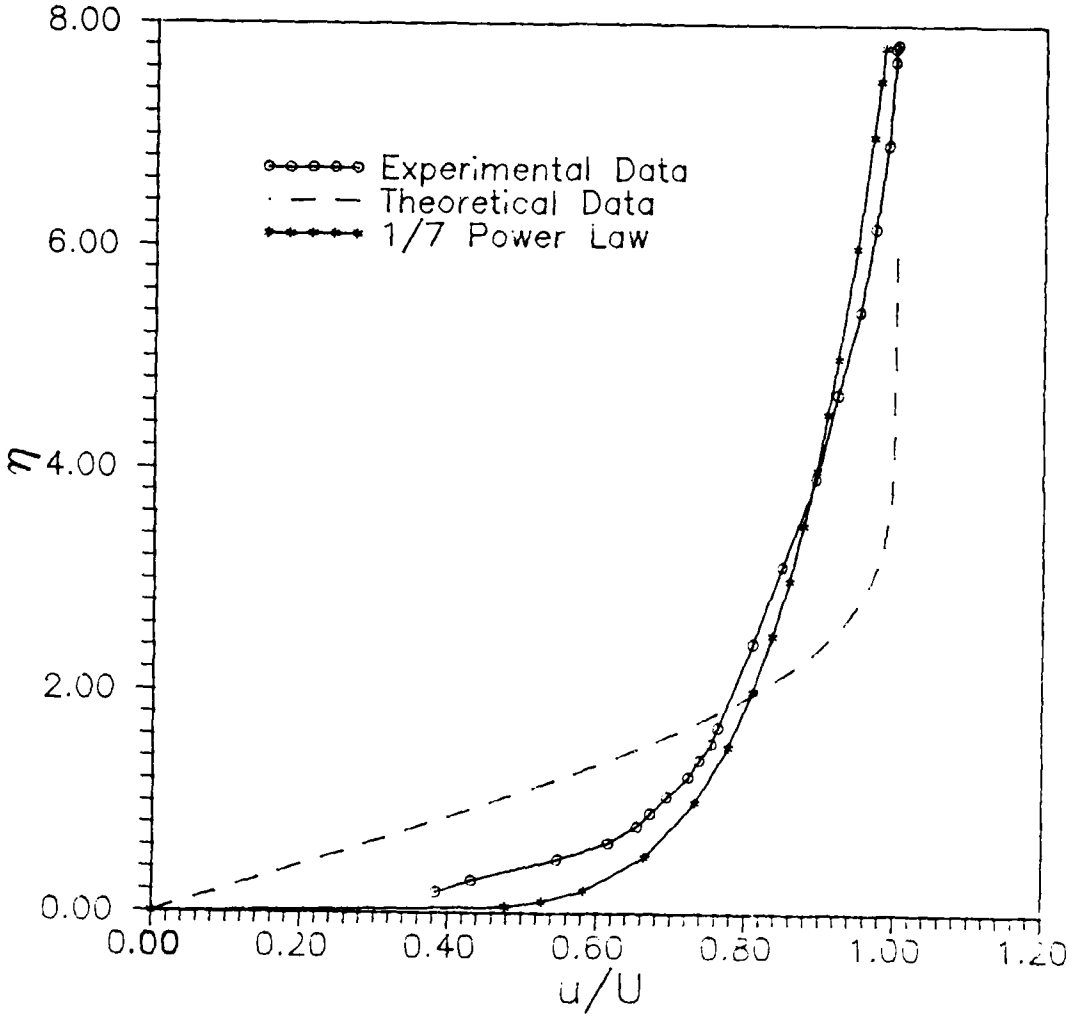

Fig. 22. Experimental Turbulent and Theoretical Laminar Boundary Layers for x = 11 in. and U = 50.376 ft/sec
(Theoretical Values from 26:265)

$$D/w = \rho U^2 \int_0^{\infty} [(u/U) - (u/U)^2] dy \quad (19)$$

where

D = drag on the surface (lbf)
w = surface width (ft)
ρ = fluid density ($slug/ft^3$)
U = freestream velocity (ft/sec)
u = local flow velocity (ft/sec)

Defining C_D in terms of the drag for flow over a flat plate results in the following equation (26:245):

$$C_D = 2D/(w \rho U^2 x) \quad (20)$$

where

C_D = drag coefficient on a plate of length x
x = horizontal location along the surface (flat plate) (ft)

Equations 19 and 20 can be combined to generate the following relationship for C_D:

$$C_D = (2/x) \int_0^{\infty} [(u/U) - (u/U)^2] dy \quad (21)$$

Equation 21 was then used to experimentally determine the C_D for any type of boundary layer on a surface. Data collection consisted of using the hot film anemometer to determine values of the local flow velocity corresponding to vertical locations throughout the entire boundary layer height (y), for a given x-location on the flat plate model. Plots of u/U versus y and $(u/U)^2$ versus y were generated from this data. Finding the area under these plotted curves provided the values of the two integral terms in Equation 21. With the area values known, the C_D corresponding to any boundary layer type was easily calculated for a particular horizontal distance (x) on the flat plate (effective flat plate length).

The accuracy of the experimentally determined C_D values was checked by comparing them to theoretically obtained numbers for flow over a flat plate. For laminar flow, the theoretical value for C_D was determined using the following equation (26:266):

$$C_D = 1.328/(Re_x)^{1/2} \tag{22}$$

where

C_D = drag coefficient
Re_x = Reynolds number, $Re_x = xU_e/\nu$

The following relationship was used to obtain the theoretical C_D value for a turbulent boundary layer (26:500):

$$C_D = 0.0303(Re_x)^{-1/7} \tag{23}$$

Table 5 shows a comparison of the experimentally and theoretically determined C_D values for both laminar and turbulent boundary layers on a flat plate. The data for laminar flow was collected at a flat plate

Table 5. C_D Values

Flow Type	Experimental C_D	Theoretical C_D	Error (%)
Laminar	0.007181	0.007189	0.111
Turbulent	0.005061	0.005068	0.138

x-location of 3 in. with a freestream velocity of 21.168 ft/sec and the turbulent flow data was taken at an x-location of 11 in. with a freestream velocity of 50.375 ft/sec.

As a result of this methodology evaluation process, experimental procedures for determining laminar and turbulent boundary layers, as well as their corresponding C_D, on a surface were derived. Future data obtained in the thesis employing these methods could now be accepted with a high degree of confidence as to their accuracy.

Appendix C: Equation Derivations

This appendix contains the detailed derivation of Equation 6 used to determine flow separation within the diffuser section as discussed previously in the Theory section. Equation 6 is an alternative form to Stratford's relationship. Repeated from Equation 5 located in the Theory section, Stratford's relationship is written as follows (3:204):

$$C_p \left[x(dC_p/dx)\right]^{1/2} (10^{-6}R_x)^{-1/10} = F(x) \qquad (5)$$

where

C_p = pressure coefficient, $C_p = 1 - (U_e/U_o)^2$
x = flow location measured from the minimum pressure point (ft)
dC_p/dx = pressure distribution
R_x = Reynolds number, $R_x = xU_e/\nu$
U_e = boundary layer edge velocity (ft/sec)
ν = kinematic viscosity (ft^2/sec)
U_o = velocity at beginning of adverse pressure gradient (ft/sec)
$F(x)$ = Stratford's criteria separation parameter

Equation 5 was simplified using the continuity equation for steady, one-dimensional incompressible fluid flow and the geometry of the diffuser. The continuity equation is written as follows:

$$A_oU_o = A_eU_e = \text{Constant} \qquad (24)$$

where

A_o = diffuser throat area per unit width at beginning of adverse pressure gradient (ft)
U_o = velocity at beginning of adverse pressure gradient (ft/sec)
A_e = diffuser area per unit width at boundary layer location (ft)
U_e = boundary layer edge velocity (ft/sec)

Using Equation 24, the following relationships were obtained:

$$A_e = (A_o U_o)/U_e \tag{25}$$

$$U_e = (A_o U_o)/A_e \tag{26}$$

A side view of the diffuser model as it appeared in the wind tunnel test section is shown in Figure 23.

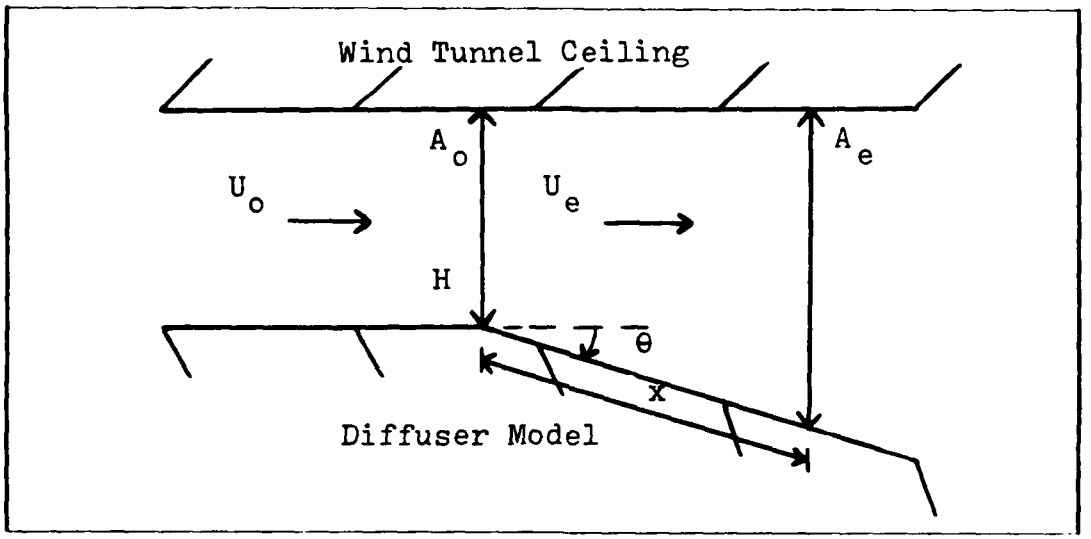

Fig. 23. Side View of the Diffuser Model in the Tunnel Test Section

Investigating the diffuser geometry portrayed above resulted in the following relationships:

$$A_e = H + x\tan\theta \tag{27}$$

$$A_o = H \tag{28}$$

$$dA_e/dx = \tan\theta \tag{29}$$

where

H = one half of the diffuser throat width (ft)
θ = one half of the diffuser divergence angle (deg)

dA_e/dx = area distribution per unit width

The above equations where then used to derive the desired form of Stratford's relationship. Recall from Equation 5 the definition of the parameter C_p: $C_p = 1 - (U_e/U_o)^2$. Taking the derivative of C_p yielded the following equation:

$$dC_p/dx = -(1/U_o^2)\ (dU_e^2/dx) \tag{30}$$

Solving for the dU_e^2/dx term in Equation 30 required the use of Equations 24 and 25 and the following steps:

$$U_e A_e = \text{Constant} \tag{24}$$

$$(U_e A_e)^2 = (\text{Constant})^2 = \text{Constant}$$

$$d(U_e A_e)^2/dx = d(\text{Constant})/dx$$

$$U_e^2(dA_e^2/dx) + A_e^2(dU_e^2/dx) = 0$$

$$2U_e^2 A_e(dA_e/dx) + A_e^2(dU_e^2/dx) = 0$$

$$U_e^2(dA_e/dx) + (A_e/2)\ (dU_e^2/dx) = 0$$

$$dU_e^2/dx = -(2U_e^2/A_e)\ (dA_e/dx)$$

$$dU_e^2/dx = -2U_e^3/(A_o U_o)\ (dA_e/dx) \tag{31}$$

Substituting Equation 31 into Equation 30 yielded the following relationship:

$$dC_p/dx = 2U_e^3/(A_o U_o^3)\ (dA_e/dx) \tag{32}$$

Substituting Equations 26, 27, 28, and 29 into Equation 32 resulted in

the following relationship for dC_p/dx:

$$dC_p/dx = 2A_o^3U_o^3/(A_oU_o^3A_e^3)\ (dA_e/dx)$$

$$dC_p/dx = (2A_o^2/A_e^3)\ (dA_e/dx)$$

$$dC_p/dx = (2\tan\theta H^2)/(H + x\tan\theta)^3 \qquad (33)$$

Substituting Equations 26, 27, and 28 into the definition of C_p produced the following formula:

$$C_p = 1 - (U_e/U_o)^2$$

$$C_p = 1 - (1/U_o^2)\ (A_o^2U_o^2/A_e^2)$$

$$C_p = 1 - H^2/(H + x\tan\theta)^2 \qquad (34)$$

Finally, substituting Equations 33 and 34 into Equation 5 yielded the form of Stratford's relationship used in this thesis to determine flow separation in the diffuser section:

$$F(x) = [1 - H^2/(H + x\tan\theta)^2][2xH^2\tan\theta/(H + x\tan\theta)^3]^{1/2}(R_x10^{-6})^{-1/10} \qquad (6)$$

Appendix D: Experimental Data

The raw experimental data is included here for completeness. It is hoped that this set of data may aid follow-on investigations.

Table 6. Experimental Data

U_{th} (ft/sec)	H (in.)	x_{sep} (in.) Plain	x_{sep} (in.) Riblets	Δx_{sep} (in.)	Δx_{sep} (%)	$\Delta x_{sep}/L$
19.0	1.75	5.0000	16.4375	11.4375	228.8	0.5446
29.0		5.6250	19.7083	14.0833	250.4	0.6706
39.0		6.1250	20.7500	14.6250	238.8	0.6964
51.0		6.4375	21.0000	14.5625	226.2	0.6935
19.0	2.25	6.6250	15.4375	8.8125	133.0	0.4196
29.0		7.0625	18.3958	11.3333	160.5	0.5397
39.0		8.0000	19.9792	11.9792	149.7	0.5704
51.0		9.0625	21.0000	11.9375	131.7	0.5685
19.0	2.75	8.5000	13.0417	4.5417	53.4	0.2163
29.0		9.4375	19.3125	9.8750	104.6	0.4702
39.0		10.5000	19.9167	9.4167	89.7	0.4484
51.0		11.4375	20.6875	9.2500	80.9	0.4405
19.0	3.25	10.2500	16.1042	5.8542	57.1	0.2788
29.0		11.6250	19.6042	7.9792	68.6	0.3800
39.0		12.6250	20.1250	7.5000	59.4	0.3571
51.0		15.4375	21.0000	5.5625	36.0	0.2649
19.0	4.25	14.4375	15.2500	0.8125	5.6	0.0387
29.0		16.8125	17.7708	0.9583	5.7	0.0456
39.0		19.7500	20.6458	0.8958	4.5	0.0427
51.0		21.0000	21.0000	0.0000	0.0	0.0000

Table 6. Experimental Data (continued)

U_{th} (ft/sec)	H (in.)	x_{sep}/L	x_{sep}/L	U_{sep} (ft/sec)	U_{sep} (ft/sec)	h^+_{sep}
		Plain	Riblets	Plain	Riblets	Plain
19.0	1.75	0.238	0.783	12.699	7.221	9.531
29.0		0.268	0.938	18.612	9.812	13.968
39.0		0.292	0.988	24.257	12.749	18.205
51.0		0.307	1.000	31.121	16.538	23.356
19.0	2.25	0.315	0.735	12.572	8.670	9.435
29.0		0.336	0.876	18.769	11.985	14.086
39.0		0.381	0.951	24.113	15.343	18.097
51.0		0.432	1.000	30.010	19.460	22.523
19.0	2.75	0.405	0.621	12.364	10.419	9.279
29.0		0.449	0.920	18.171	13.066	13.637
39.0		0.500	0.948	23.451	17.275	17.600
51.0		0.545	0.985	29.613	22.113	22.225
19.0	3.25	0.488	0.767	12.277	10.213	9.214
29.0		0.554	0.934	17.889	14.164	13.426
39.0		0.601	0.958	23.290	18.793	17.479
51.0		0.735	1.000	27.948	24.034	20.975
19.0	4.25	0.688	0.726	11.950	11.706	8.969
29.0		0.801	0.846	17.191	16.801	12.902
39.0		0.940	0.983	21.583	21.155	16.198
51.0		1.000	1.000	27.448	27.448	20.600

Table 6. Experimental Data (continued)

U_{th} (ft/sec)	H (in.)	D_H (th) (in.)	Re_{th} (10^4)	D_H (sep) (in.) Plain	Re_{sep} (10^4) Plain	D_H (sep) (in.) Riblets	Re_{sep} (10^4) Riblets
19.0	1.75	2.792	2.631	3.796	2.391	5.523	1.978
29.0			4.016	3.909	3.609	5.913	2.878
39.0			5.401	3.997	4.810	6.029	3.813
51.0			7.063	4.052	6.255	6.056	4.968
19.0	2.25	3.393	3.198	4.556	2.841	5.751	2.473
29.0			4.881	4.623	4.304	6.086	3.618
39.0			6.565	4.765	5.700	6.254	4.760
51.0			8.585	4.921	7.325	6.359	6.138
19.0	2.75	3.933	3.706	5.242	3.215	5.808	3.002
29.0			5.657	5.365	4.836	6.477	4.198
39.0			7.608	5.501	6.399	6.536	5.601
51.0			9.949	5.617	8.251	6.609	7.250
19.0	3.25	4.419	4.164	5.818	3.543	6.445	3.265
29.0			6.356	5.975	5.302	6.775	4.760
39.0			8.548	6.085	7.030	6.821	6.359
51.0			11.180	6.379	8.843	6.898	8.224
19.0	4.25	5.260	4.957	6.828	4.047	6.899	4.006
29.0			7.567	7.032	5.997	7.111	5.926
39.0			10.180	7.269	7.782	7.338	7.700
51.0			13.310	7.365	10.030	7.365	10.030

Vita

Captain Nathan W. Martens was born [redacted]

He graduated from Winston Churchill High School, San Antonio, Texas, in 1979 and attended the United States Air Force Academy, where he earned the degree of Bachelor of Science in Aeronautical Engineering and a regular commission in the USAF. Upon graduation, he was assigned to the Air Force Wright Aeronautical Laboratories, Wright-Patterson AFB, as an Aircraft Design Engineer until entering the School of Engineering, Air Force Institute of Technology, in June of 1987.

[redacted]

UNCLASSIFIED
SECURITY CLASSIFICATION OF THIS PAGE

REPORT DOCUMENTATION PAGE

Form Approved
OMB No. 0704-0188

1a. REPORT SECURITY CLASSIFICATION UNCLASSIFIED	1b. RESTRICTIVE MARKINGS
2a. SECURITY CLASSIFICATION AUTHORITY	3. DISTRIBUTION/AVAILABILITY OF REPORT Approved for public release; distribution unlimited
2b. DECLASSIFICATION/DOWNGRADING SCHEDULE	
4. PERFORMING ORGANIZATION REPORT NUMBER(S) AFIT/GAE/AA/88D-23	5. MONITORING ORGANIZATION REPORT NUMBER(S)
6a. NAME OF PERFORMING ORGANIZATION School of Engineering 6b. OFFICE SYMBOL (If applicable) AFIT/ENY	7a. NAME OF MONITORING ORGANIZATION
6c. ADDRESS (City, State, and ZIP Code) Air Force Institute of Technology (AU) Wright-Patterson AFB OH 45433-6583	7b. ADDRESS (City, State, and ZIP Code)
8a. NAME OF FUNDING/SPONSORING ORGANIZATION 8b. OFFICE SYMBOL (If applicable)	9. PROCUREMENT INSTRUMENT IDENTIFICATION NUMBER
8c. ADDRESS (City, State, and ZIP Code)	10. SOURCE OF FUNDING NUMBERS PROGRAM ELEMENT NO. / PROJECT NO. / TASK NO / WORK UNIT ACCESSION NO.

11. TITLE (Include Security Classification)
EFFECT OF RIBLETS UPON FLOW SEPARATION IN A SUBSONIC DIFFUSER (U)

12. PERSONAL AUTHOR(S)
Nathan W. Martens, Capt, USAF

13a. TYPE OF REPORT	13b. TIME COVERED	14. DATE OF REPORT (Year, Month, Day)	15. PAGE COUNT
MS Thesis	FROM _____ TO _____	1988 December	101

16. SUPPLEMENTARY NOTATION

17. COSATI CODES			18. SUBJECT TERMS (Continue on reverse if necessary and identify by block number)
FIELD	GROUP	SUB-GROUP	Riblets Subsonic Diffuser Flow Separation
01	01		

19. ABSTRACT (Continue on reverse if necessary and identify by block number)

Thesis Advisor: Lt Col Paul I. King
Associate Professor
Department of Aeronautics and Astronautics

Abstract on back.

12 Jan 1989

20. DISTRIBUTION/AVAILABILITY OF ABSTRACT ☐ UNCLASSIFIED/UNLIMITED ☒ SAME AS RPT. ☐ DTIC USERS	21. ABSTRACT SECURITY CLASSIFICATION UNCLASSIFIED
22a. NAME OF RESPONSIBLE INDIVIDUAL Lt Col Paul I. King, Assoc. Professor	22b. TELEPHONE (Include Area Code) (513) 255-3517 22c. OFFICE SYMBOL AFIT/ENY

DD Form 1473, JUN 86 — Previous editions are obsolete. — SECURITY CLASSIFICATION OF THIS PAGE
UNCLASSIFIED

UNCLASSIFIED

The objective of this thesis was to investigate the effect of riblets upon flow separation in a two-dimensional straight-walled subsonic diffuser. Riblets are small flow-aligned grooves which can be attached to an aerodynamic body. Studies involving the application of riblets to turbulent flow over a flat plate have consistently shown a decrease in viscous drag as compared to the same surface without riblets. The purpose of this investigation was to determine the effect applying riblets to the walls of a subsonic diffuser would have upon flow separation in the fluid handling device.

For this investigation, it was found flow separation was indeed delayed in a diffuser employing riblets as compared to a geometrically identical plain diffuser. For the smaller throat widths, this delay was significant, being as high as 250% due to riblets. As the diffuser throat width increased, the delay in flow separation due to riblets decreased. Also evident in the investigation was the strong dependence of flow separation upon throat velocity for the diffuser with riblets.

END
DATE
FILMED
3-89
DTIC